Improved Productivity and Stability for CO_2 Hydrogenation Using Pincer Ligated Mn Complexes with Hemilabile Ligands

Justin C. Wedal,[1,3] Kyler B. Virtue[2] Wesley H. Bernskoetter,[2,*] Nilay Hazari,[1,4,**] Brandon Q. Mercado,[1] and Nicole Piekut[1]

[1]The Department of Chemistry, Yale University, P. O. Box 208107, New Haven, Connecticut, 06520, USA.

[2]The Department of Chemistry, The University of Missouri, Columbia, Missouri, 65211, USA.

[3]These authors contributed equally.

[4]Lead contact.

*Correspondence: bernskoetterwh@missouri.edu

**Correspondence: nilay.hazari@yale.edu

Summary: Pincer ligands are widely used to support transition metal catalysts, but first-row systems often deactivate too quickly for widespread use. Here, pincer ligands bearing an additional hemilabile donor were designed to stabilize Mn catalysts for CO_2 hydrogenation to formate. Ligands of the type $(RCH_2CH_2)N(CH_2CH_2P^iPr_2)_2$ ($^{iPr}PN^RP$; R = OMe, CH_2OMe, NMe_2, P^iPr_2) were synthesized and coordinated to Mn to form complexes of the type $(^{iPr}PN^RP)Mn(CO)_2H$. Their performance was compared to $\{MeN(CH_2CH_2P^iPr_2)_2\}Mn(CO)_2H$, which lacks a pendant donor. The pendant donor identity and arm length strongly influenced catalytic activity, but all pendant arm containing systems extended catalyst lifetime. Notably, $(^{iPr}PN^{CH2OMe}P)Mn(CO)_2H$ achieved turnover frequencies of 158,000 h^{-1} and turnover numbers of 838,000, exceeding most state-of-the-art catalysts. Mechanistic studies revealed that hemilabile coordination enhances stability by avoiding deactivation, although excessive binding can lead to inactive states. This work demonstrates hemilabile donors dramatically improve pincer-based Mn catalysts and provides design principles for broader applications.

Keywords: Manganese, pincer ligands, hemilabile ligands, catalysis, CO_2 hydrogenation, formate mechanistic studies.

Introduction

Carbon dioxide (CO_2) is an attractive chemical feedstock because it is an inexpensive, non-toxic, and environmentally damaging waste product generated on a large scale.[1] The hydrogenation of CO_2 to produce formic acid (or formate salts) is of particular interest since approximately one million tons of formic acid are produced annually from non-renewable fossil-fuel derived feedstocks (Figure 1a).[2] Further, formic acid could be used as a liquid organic hydrogen carrier, but sustainable synthetic methods are needed for this approach to be environmentally beneficial.[3] In principle, the catalytic generation of formic acid (or formate salts) using H_2 produced via electrolysis with renewably sourced electricity and CO_2 could solve this challenge.[4]

Homogeneous catalysts based on precious metals such as Ir,[5] Rh,[6] Pd,[7] and Ru[8] are known to hydrogenate CO_2 to formate (see Supporting Information, Section S1 for a comprehensive list of catalysts). However, even though systems based on Ir and Ru typically give the highest activity and productivity, their high cost, limited abundance, and relative toxicity provides motivation for the discovery of catalysts based on more abundant first-row transition metals.[9] Complexes based

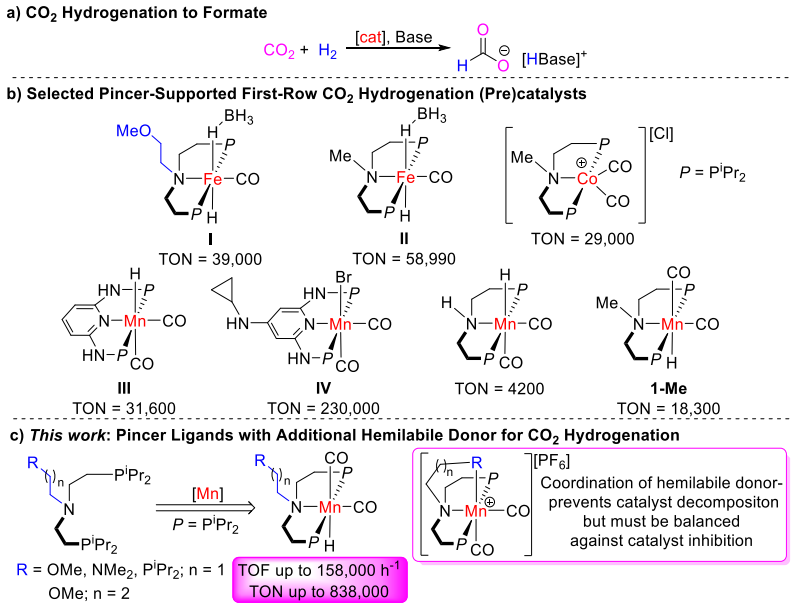

Figure 1: a) Generic equation for CO_2 hydrogenation to formate. **b**) Selected pincer ligated first-row catalysts for CO_2 hydrogenation and associated maximum turnover number (TON) regardless of conditions. **c**) *This work*: Pincer ligands with an additional hemilabile donor result in highly active and productive Mn catalysts for CO_2 hydrogenation to formate.

on Cr,[10] Mn,[11] Fe,[12] Co,[13] Ni,[14] and Cu[15] are all active catalysts for CO_2 hydrogenation to formate. PNP pincer ligands are commonly used to support the most active and productive Mn, Fe, and Co catalysts (Figure 1b). Therefore, significant research effort has focused on tuning the electronic and steric properties of PNP ligands, mostly by altering the substituents on the P and N donors, which has led to improvements in catalytic performance.[9a] Nevertheless, the majority of first-row metal catalysts undergo more facile catalyst deactivation compared to their Ru and Ir congeners.[2b,12d,16] These observations suggest that modifications to PNP pincer ligands that lead to improved catalyst lifetimes would be impactful in advancing base metal catalysis. For many PNP pincer metal catalysts,[2b,16] catalyst deactivation occurs via a bimetallic pathway with coordinatively unsaturated species serving as key intermediates. Therefore, one potential strategy to prevent catalyst decomposition is the use of hemilabile ligands.

The term "hemilabile ligand" was introduced by Jeffrey and Rauchfuss in 1979 and describes a chelating ligand which contains a weak donor group that readily undergoes ligand substitution.[17] These hemilabile donors can stabilize key intermediates by binding to the metal center, but if designed correctly, can be readily displaced by a substrate to enable the desired reactivity. Metal catalysts with hemilabile ligands can facilitate a variety of catalytic reactions including (de)hydrogenation, (de)carbonylation, hydroformylation, alkene metathesis, polymerization, and cross-coupling and are used in chemical sensing.[18] Some proteins also make use of hemilabile donors to switch between resting and active states using allostery.[19] The majority of catalysts with hemilabile ligands fluctuate between monodentate (κ^1) and bidentate (κ^2) or bidentate and tridentate (κ^3) coordination modes and there are few studies exploring the addition of hemilabile donors to pincer ligands.[20] Further, most of the studies with pincer ligands focus on the impact of the hemilabile ligand on coordination chemistry, as opposed to effects on catalysis. We hypothesized that the development of PNP pincer ligands with an additional hemilabile donor could stabilize first-row transition metal catalysts for CO_2 hydrogenation by preventing decomposition of coordinatively unsaturated intermediates and lead to more productive systems.

We recently prepared the $MeOCH_2CH_2N(CH_2CH_2P^iPr_2)_2$ ($^{iPr}PN^{2OMe}P$) ligand containing a hemilabile ether donor linked by a two-carbon bridge and coordinated it to Fe (**I**, Figure 1b).[21] Complex **I** was an active catalyst for CO_2 hydrogenation to formate and gave increased lifetimes compared to analogous Fe catalysts bearing the widely studied tridentate $MeN(CH_2CH_2P^iPr_2)_2$ ($^{iPr}PN^{Me}P$) ligand (**II**, Figure 1b).[12d] **I** and **II** displayed similar overall turnover numbers (TONs)

of *ca* 40,000 under directly comparable conditions,[22] but **I** gave significantly lower turnover frequencies (TOFs). This TON is lower than the value for **I** of 58,990 shown in Figure 1, which was collected under slightly different conditions. We proposed that the TOF for **I** was inhibited by coordination of the hemilabile ether donor and the improved catalyst longevity was insufficient to provide an increase in TON over extended reaction times. This suggested that by varying the pendant donor and/or the length of the linker between the PNP ligand and the hemilabile donor, it would be possible to improve catalytic performance by attenuating the binding strength of the pendant arm. Here, the synthesis of $^{iPr}PN^{R}P$ pincer ligands with hemilabile ether, amine, and phosphine donors is described (Figure 1c). The ligands were coordinated to Mn because prior reports indicate that Mn complexes generate some of the most productive pincer ligated first-row transition metal complexes.[11d] The identity of the hemilabile donor directly impacts catalytic performance for CO_2 hydrogenation to formate and the additional donor can stabilize the catalyst by weakly binding to the Mn center. By carefully selecting the hemilabile substituent and linker length, we describe a Mn catalyst that can give a TOF of up to 158,000 h^{-1} and a TON of up to 838,000 for CO_2 hydrogenation to formate. These are among the highest numbers reported for molecular catalysts based on either first-row or precious metals and validate our hypothesis that the identity of the hemilabile substituent can be used to improve catalytic performance. We expect this general strategy, as well as the ligands described in this work, will be valuable for developing improved pincer-ligated catalysts for a variety of transformations.

Results and Discussion

Synthesis of PNP Ligands with an Additional Hemilabile Donor and Associated Mn Complexes

Based on our success increasing the lifetime of Fe catalysts for CO_2 hydrogenation using the $^{iPr}PN^{2OMe}P$ ligand,[21] we aimed to synthesize pincer ligands containing different pendant hemilabile donors and linker lengths to support complexes with improved catalytic performance. In addition to $^{iPr}PN^{2OMe}P$, we targeted three ligands: (i) $MeOCH_2CH_2CH_2N(CH_2CH_2P^iPr_2)_2$ ($^{iPr}PN^{3OMe}P$) which contains a three-carbon linker between the nitrogen atom of the pincer ligand and the hemilabile donor. This was expected to change the binding strength of the hemilabile donor compared to $^{iPr}PN^{2OMe}P$ by forming a six instead of a five-membered ring upon coordination of the pendant arm. (ii) $Me_2NCH_2CH_2N(CH_2CH_2P^iPr_2)_2$ ($^{iPr}PN^{NMe2}P$) which contains an additional amine donor. The change in donor was expected to alter the binding strength of the pendant arm compared to $^{iPr}PN^{2OMe}P$. (iii) $^iPr_2PCH_2CH_2N(CH_2CH_2P^iPr_2)_2$ ($^{iPr}PN^{PiPr2}P$), a previously reported[20e]

symmetric ligand containing three equivalent P donors, which in principle could all bind tightly to the metal center.

Our general synthetic strategy followed a three-step protocol (Figure 2) modified from that used previously for $^{iPr}PN^{2OMe}P$ involving:[21] (i) an S_N2 reaction between diethanolamine and a pendant arm precursor containing a chloride leaving group,[20d,23] (ii) chlorination of the hydroxyl groups with thionyl chloride,[20d,23] and (iii) substitution of the chloride groups with $P^iPr_2^-$ to afford the final ligand of the form $^{iPr}PN^{R}P$.[24] A weakness in our previous synthesis of $^{iPr}PN^{2OMe}P$ was the low yield in the initial S_N2 reaction between 1-chloro-2-methoxyethane and diethanolamine, which we improved in this work by altering the reaction conditions.[21] This methodology was used to successfully prepare $^{iPr}PN^{2OMe}P$ and $^{iPr}PN^{3OMe}P$ in overall yields of 22% and 38%, respectively (Figure 2a).

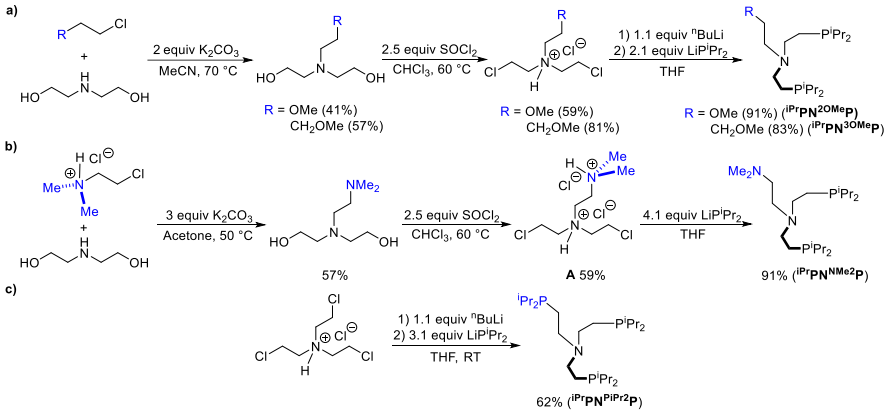

Figure 2: Syntheses of pendant arm containing pincer ligands. **a)** $^{iPr}PN^{2OMe}P$ and $^{iPr}PN^{3OMe}P$, **b)** $^{iPr}PN^{NMe2}P$, and **c)** $^{iPr}PN^{PiPr2}P$.

A slight modification was required in the final step of the synthesis of $^{iPr}PN^{NMe2}P$ (Figure 2b). The reaction of the dicationic intermediate **A** with ^{n}BuLi did not lead to the formation of the desired free-based amine. Instead, the free amine likely underwent an intramolecular reaction to generate an activated piperazine, which reacted further with ^{n}BuLi (see SIIIc).[25] To prevent this problem, LiP^iPr_2 was used to free-base intermediate **A** and this led to the formation of $^{iPr}PN^{NMe2}P$ in 31% overall yield. $^{iPr}PN^{PiPr2}P$ was synthesized in one step from commercially available tris(chloroethyl)amine hydrochloride, ^{n}BuLi, and LiP^iPr_2 (Figure 2c). All the ligands are air sensitive and were characterized using multinuclear NMR spectroscopy and high-resolution mass

spectrometry (see SIIIa).

Mn hydrides of the type (^{iPr}PN^{R}P)Mn(CO)$_2$H (**1-R**) were initially targeted to evaluate the catalytic performance of our series of ^{iPr}PN^{R}P ligands. Our synthetic route was a modified version of the procedure previously used to access the CO_2 hydrogenation catalyst (^{iPr}PN^{Me}P)Mn(CO)$_2$H (**1-Me**).[26] Initially, our pincer ligands were heated at 100 °C in toluene solutions with Mn(CO)$_5$Br to generate (^{iPr}PN^{R}P)Mn(CO)$_2$Br species in good yields (Figure 3a).[27] As was observed for related PNP-ligated Mn halide complexes without a pendant arm,[11e] NMR spectral signals for the

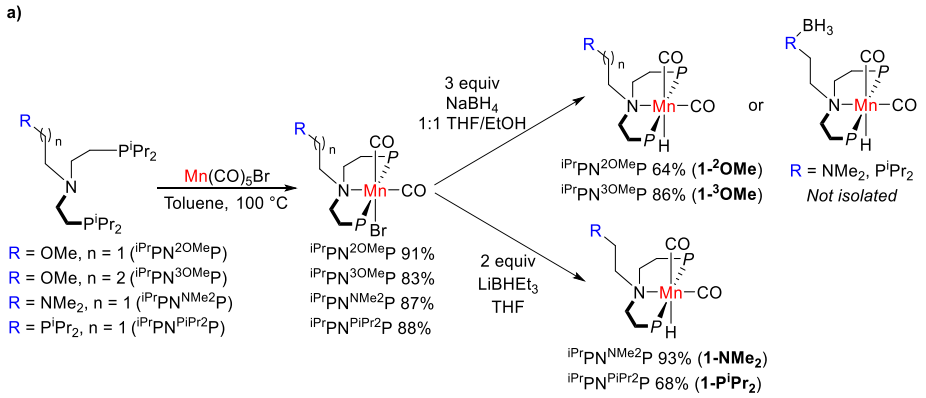

Figure 3: a) Synthesis of Mn hydride complexes with PNP pincer ligands with a hemilabile donor. **b)** Molecular structures of (^{iPr}PN^{2OMe}P)Mn(CO)$_2$Br (left) and (^{iPr}PN^{3OMe}P)Mn(CO)$_2$H (right), **1-^{3}OMe**. Ellipsoids at 50%. Hydrogen atoms except hydrides are omitted for clarity. Selected bond lengths (Å) and angles (°) for (^{iPr}PN^{2OMe}P)Mn(CO)$_2$Br: Mn(1)-P(1) 2.2996(15), Mn(1)-P(2) 2.3000(14), Mn(1)-N(1) 2.226(4), Mn(1)-Br1 2.5603(10), Mn(1)-C(20) 1.819(9), Mn(1)-C(21) 1.761(6); P(1)-Mn(1)-P(2) 166.66(6), P(1)-Mn(1)-N(1) 83.52(11), P(1)-Mn(1)-Br(1) 89.82(4), P(1)-Mn(1)-C(20) 89.63(17), P(1)-Mn(1)-C(21) 96.36(17), P(2)-Mn(1)-N(1) 83.52(11), P(2)-Mn(1)-Br(1) 86.65(4), P(2)-Mn(1)-C(20) 94.71(17), P(2)-Mn(1)-C(21) 96.53(17), N(1)-Mn(1)-Br(1) 88.21(11), N(1)-Mn(1)-C(20) 95.5(2), N(1)-Mn(1)-C(21) 178.8(2). Selected bond lengths (Å) and angles (°) for **1-^{3}OMe**: Mn(1)-P(1) 2.2355(10), Mn(1)-P(2) 2.2449(11), Mn(1)-N(1) 2.217(3), Mn(1)-C(1) 1.770(4), Mn(1)-C(2) 1.753(4); P(1)-Mn(1)-P(2) 163.85(4), P(1)-Mn(1)-N(1) 83.87(8), P(2)-Mn(1)-N(1) 82.77(8), P(1)-Mn(1)-C(1) 93.32(12), P(1)-Mn(1)-C(2) 95.62(12), P(2)-Mn(1)-C(1) 98.08(12), P(2)-Mn(1)-C(2) 96.34(13), N(1)-Mn91)-C(1) 100.96(14), N(1)-Mn(1)-C(2) 171.97(15), C(1)-Mn(1)-C(2) 87.07(17).

complexes were broad (see SIIIe for an extended discussion). ^{31}P NMR spectroscopy indicated that the complexes exist as two isomers with an approximate ratio of 9:1. The isomers of (^{iPr}PN^{R}P)Mn(CO)$_2$Br were assigned as differing in the configuration of the Mn-Br bond with respect to the substituent on the N donor, either on the same or opposite face of the PNP plane. The same isomeric variation was previously described in related pincer Mn complexes.[11e,26] Two strong CO stretches were observed in the IR spectra of each species and the solid-state structures of (^{iPr}PN^{2OMe}P)Mn(CO)$_2$Br, (^{iPr}PN^{NMe2}P)Mn(CO)$_2$Br, and (^{iPr}PN^{PiPr2}P)Mn(CO)$_2$Br were determined using X-ray diffraction (see Figure 3b and SI). The complexes display distorted octahedral geometries around the Mn center with the ^{iPr}PN^{R}P ligand binding in the expected meridional fashion. The Br ligand is on the opposite side to the N substituent of the ^{iPr}PN^{R}P ligand. The geometrical parameters around Mn are comparable among all three complexes and similar to related (PNP)Mn(CO)$_2$Br complexes in the literature.[11e,26,28] This indicates the identity of the non-coordinated pendant arm has little inductive or steric impact on the Mn center.

Reactions of (^{iPr}PN^{2OMe}P)Mn(CO)$_2$Br or (^{iPr}PN^{3OMe}P)Mn(CO)$_2$Br with NaBH$_4$ in a 1:1 mixture of THF/EtOH afforded (^{iPr}PN^{2OMe}P)Mn(CO)$_2$H (**1-^{2}OMe**) or (^{iPr}PN^{3OMe}P)Mn(CO)$_2$H (**1-^{3}OMe**), respectively, in good yields (Figure 3a). However, reactions of (^{iPr}PN^{R}P)Mn(CO)$_2$Br (R = NMe$_2$, P^{i}Pr$_2$) with NaBH$_4$ led to trapping of the BH$_3$ by-product by the pendant donor and formation of (^{iPr}PN$^{R•BH3}$P)Mn(CO)$_2$H. The borane could be liberated from (^{iPr}PN$^{NMe2•BH3}$P)Mn(CO)$_2$H via reaction with NEt$_3$ to generate the desired product (^{iPr}PN^{NMe2}P)Mn(CO)$_2$H (**1-NMe$_2$**), but the two step-process proved cumbersome. Treatment of (^{iPr}PN$^{PiPr2•BH3}$P)Mn(CO)$_2$H with NEt$_3$ did not result in liberation of BH$_3$. This is consistent with phosphines being a better Lewis base for BH$_3$ than amines, which was supported by DFT calculations (see SVI). Complexes **1-NMe$_2$** and (^{iPr}PN^{PiPr2}P)Mn(CO)$_2$H (**1-P^{i}Pr$_2$**) were successfully prepared using LiBHEt$_3$ as the hydride source instead of NaBH$_4$ (Figure 3a). Analysis using ^{11}B NMR spectroscopy confirmed that the BEt$_3$ by-product does not coordinate to the pendant donor.

The ^{1}H and ^{31}P NMR spectra of the (^{iPr}PN^{R}P)Mn(CO)$_2$H complexes obtained prior to purification exhibit signals for two isomers in various ratios depending on the pendant arm identity. Similar to the Mn bromide complexes, these isomers likely differ in the relative orientation of the Mn-H bond with respect to the pendant arm. In some cases, such as for **1-^{2}OMe** and **1-^{3}OMe**, crystallization from hexane at −35 °C afforded a single isomer. In the ^{1}H NMR spectra of the crystallized complexes, resonances assigned to the Mn hydride were observed at approximately

−5 ppm. Interestingly, the NMR spectra of **1-R** are sharp in contrast to those of the Mn bromide analogues (see SIIIe for further discussion). DFT calculations determined that the isomer with the Mn-H bond on the opposite side of the ^{iPr}PNP ligand plane as the pendant arm is preferred by 2.1 kcal mol^{-1} for **1-^{2}OMe** but the isomers are similar in energy for **1-^{3}OMe** (see SVI). The IR spectra of **1-R** display two characteristic CO bands around 1880 and 1805 cm^{-1}. These peaks are shifted to lower energy compared to (^{iPr}PN^{R}P)Mn(CO)$_2$Br complexes, consistent with increased electron donation from the hydride ligand. The solid-state structures of **1-^{2}OMe** and **1-^{3}OMe** reveal a distorted octahedral geometry about the Mn (Figure 3b and SVII). The complexes have slightly shorter Mn-P distances than the bromide analogs, but similar Mn-N and Mn-CO distances. The P-Mn-P angles in both structures are slightly more acute and the P-Mn-N slightly larger than the bromide analogs. The bond distances and angles are similar to those observed in **1-Me**,[26] again suggesting that when the pendant arm is not coordinated, it has minimal effect on the Mn center.

Our pincer ligands were designed so that the pendant donor could potentially stabilize coordinatively unsaturated species during catalysis by coordinating to the metal center. To probe the ability of the pendant ether donor to coordinate, **1-^{2}OMe** and **1-^{3}OMe** were treated with lutidinium hexafluorophosphate (Figure 4a). This resulted in the liberation of H_2 and the formation of the complexes [(κ^4-^{iPr}PN^{2OMe}P)Mn(CO)$_2$][PF$_6$] (**2-^{2}OMe**) or [(κ^4-^{iPr}PN^{3OMe}P)Mn(CO)$_2$][PF$_6$] (**2-^{3}OMe**). A slight excess of the Mn complex was utilized to aid in purification, as separation of residual lutidinium hexafluorophosphate was challenging. Two resonances were observed in the ^{31}P NMR spectra of **2-^{2}OMe** and **2-^{3}OMe**. The peaks at 80.38 ppm for **2-^{2}OMe** and 76.60 ppm for

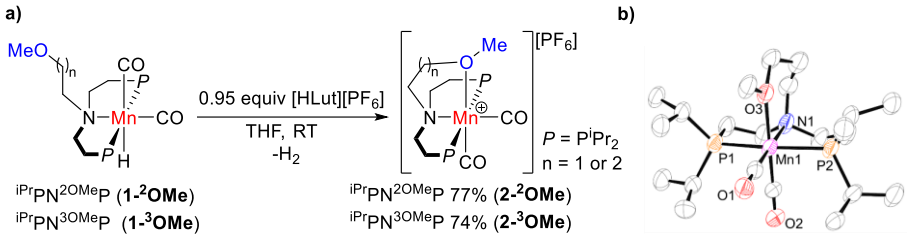

Figure 4: a) Synthesis of Mn complexes with the pendant arm on the pincer ligand bound. **b)** Solid-state structure of **2-^{3}OMe**. Ellipsoids at 35%. Hydrogen atoms, disorder, and the PF$_6$ counterion are omitted for clarity. Selected bond lengths (Å) and angles (°) for **2-^{3}OMe**: Mn(1)-P(1) 2.310(2), Mn(1)-P(2) 2.303(2), Mn(1)-N(1) 2.181(5), Mn(1)-O(3) 2.180(5), Mn(1)-C(1) 1.768(7), Mn(1)-C(2) 1.763(9); P(1)-Mn(1)-P(2) 168.55(8), P(1)-Mn(1)-N(1) 84.09(17), P(2)-Mn(1)-N(1) 84.64(17), P(1)-Mn(1)-O(3) 92.93(12), P(2)-Mn(1)-O(3) 89.13(13), P(1)-Mn(1)-C(1) 95.7(2), P(1)-Mn(1)-C(2) 88.4(2), P(2)-Mn(1)-C(1) 95.5(2), P(2)-Mn(1)-C(2) 90.0(2), N(1)-Mn(1)-O(3) 90.4(2), N(1)-Mn(1)-C(1) 178.5(3), N(1)-Mn(1)-C(2) 91.7(3), O(3)-Mn(1)-C(1) 91.1(3), O(3)-Mn(1)-C(2) 177.6(3), C(1)-Mn(1)-C(2) 86.8(3).

2-^{3}OMe were assigned to the $^{iPr}PN^RP$ ligand, while a peak at −144 ppm was assigned to the PF_6 anion. The IR spectrum showed two strong absorption bands in the CO region, which were blue shifted compared to ($^{iPr}PN^RP$)Mn(CO)$_2$Br and **1-R**, as expected for a cationic complex. The ^{1}H NMR data revealed only slight changes to the chemical shift of the protons associated with the pendant methoxy group compared to the starting materials, making it challenging to definitively state that coordination of the pendant arm had occurred using NMR spectroscopy. However, the solid-state structures of **2-^{2}OMe** and **2-^{3}OMe** established coordination of the pendant ether arm (Figure 4b and SVI). The $^{iPr}PN^{2OMe}P$ or $^{iPr}PN^{3OMe}P$ ligand is bound in a tetradentate (κ^4) fashion, with the N donor and pendant ether arm each *trans* to a CO ligand. The change from κ^3 to κ^4 coordination mode results in slightly longer Mn-N distances and larger P-Mn-P angles compared to ($^{iPr}PN^RP$)Mn(CO)$_2$Br or ($^{iPr}PN^RP$)Mn(CO)$_2$H, although the cationic charge of **2-^{2}OMe** or **2-^{3}OMe** complicates the comparison. The bond distances between the Mn and pendant ether donor, 2.13(3) Å for **2-^{2}OMe** and 2.180(5) Å for **2-^{3}OMe**, are in the range typically observed for dative Mn–O bonds.[29] While **2-^{2}OMe** was stable in solution and the solid-state for days, **2-^{3}OMe** slowly converted to the tricarbonyl species [($^{iPr}PN^{3OMe}P$)Mn(CO)$_3$][PF_6] (**3-^{3}OMe**, *vide infra*) and free $^{iPr}PN^{3OMe}P$ ligand. This process occurred over days in the solid-state at −35 °C and over hours at ambient temperature in C_6D_6 solution (see SVg). Separation of **2-^{2}OMe** and **3-^{3}OMe** was difficult and consequently, we were unable to isolate **2-^{3}OMe** on preparative scale in pure form. These observations suggest that the binding of the pendant arm in **2-^{3}OMe** is weaker than for **2-^{2}OMe** and are consistent with the longer Mn–O bond distance in **2-^{3}OMe**.

In **2-^{2}OMe** and **2-^{3}OMe**, the pendant arm binds in the coordination site formerly occupied by the CO ligand *trans* to the hydride in **1-^{2}OMe** and **1-^{3}OMe**. This indicates a geometric rearrangement accompanies the protonation reaction. Two potential pathways for the rearrangement are: (i) protonation could lead to a coordinatively unsaturated cationic five-coordinate intermediate. Intramolecular rearrangements, such as Berry pseudorotations, are typically facile for five-coordinate complexes and this could facilitate the change in the relative positions of the ligands. (ii) The protonation reaction could occur selectively from a less thermodynamically favored isomer with the pendant arm on the same side of the PNP plane as the Mn-H bond. This pathway is less likely because although we observe interconversion between the *syn* and *anti*-isomers of **1-^{3}OMe** (see SVe), this occurs on a slower timescale than the protonation reaction. Nevertheless, it is possible that lutidinium increases the rate of isomerization. The exact

mechanism for the geometric rearrangement is not clear at this stage, but our observations suggest that the pendant donor can coordinate to vacant sites potentially generated on the other side of the PNP ligand plane to the unbound pendant arm.

As described above, the tricarbonyl species **3-^{3}OMe** was always observed in samples of **2-^{3}OMe**. Authentic samples of [(^{iPr}PN^{R}P)Mn(CO)$_3$][PF$_6$] (R = ^{2}OMe, ^{3}OMe, Me) were prepared by treatment of (^{iPr}PN^{R}P)Mn(CO)$_2$Br with AgPF$_6$ under 1 atm of CO in THF (Figure 5a and SIIIb). Notably, related cationic carbonyl species have been proposed as catalyst deactivation products in CO_2 hydrogenation using ^{iPr}PN^{R}P ligated Fe catalysts.[16d,21] **3-^{2}OMe**, **3-^{3}OMe**, and **3-Me** were characterized using NMR and IR spectroscopy (see SIIIb). **3-^{2}OMe** was not isolated as a bulk material as exposure to vacuum led to CO loss and the formation of **2-^{2}OMe**, demonstrating that binding of the pendant arm can stabilize the Mn complex following ligand loss. The solid-state structures of **3-^{2}OMe** (Figure 5b) and **3-Me** (see SVII) were determined by X-ray diffraction and display similar metrical parameters around Mn to those of **2-^{2}OMe**. This is somewhat surprising given that ^{iPr}PN^{2OMe}P binds in a κ^4-fashion in **2-^{2}OMe** and a κ^3-fashion in **3-^{2}OMe** but is likely because both species are six-coordinate cationic complexes.

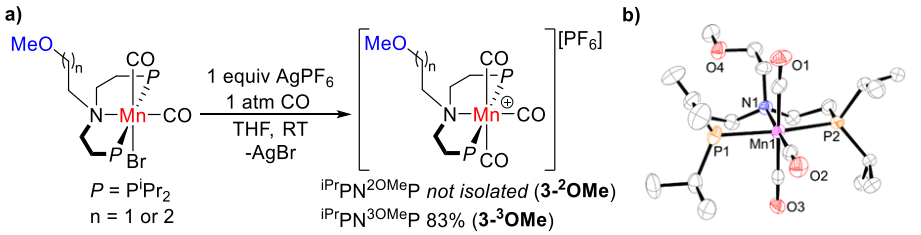

Figure 5: a) Synthesis of [(^{iPr}PN^{R}P)Mn(CO)$_3$][PF$_6$] (**3-R**). **b)** Solid-state structure of **3-^{2}OMe**. Ellipsoids at 50%. Hydrogen atoms, disordered atom positions, and the PF$_6$ counterion are omitted for clarity. Selected bond lengths (Å) and angles (°) for **3-^{2}OMe**: Mn(1)-P(1) 2.3113(9), Mn(1)-P(2) 2.3081(9), Mn(1)-N(1) 2.184(2), Mn(1)-C(1) 1.848(3), Mn(1)-C(2) 1.785(3), Mn(1)-C(3) 1.831(3); P(1)-Mn(1)-P(2) 166.44(3), P(1)-Mn(1)-N(1) 83.28(7), P(2)-Mn(1)-N(1) 83.22(7), P(1)-Mn(1)-C(1) 91.66(10), P(1)-Mn(1)-C(2) 97.03(10), P(1)-Mn(1)-C(3) 88.16(9), P(2)-Mn(1)-C(1)90.64(10), P(2)-Mn(1)-C(2) 96.46(10), P(2)-Mn(1)-C(3) 91.06(9), N(1)-Mn(1)-C(1) 94.38(10), N(1)-Mn(1)-C(2) 179.69(12), N(1)-Mn(1)-C(3) 92.12(10), C(1)-Mn(1)-C(2) 85.62(12), C(1)-Mn(1)-C(3) 173.43(12), C(2)-Mn(1)-C(3) 87.88(12).

Overall, based on our synthetic results, it is clear that the ^{iPr}PN^{R}P pincer ligands with pendant donors support Mn hydride complexes analogous to the more widely studied PNP versions without additional hemilabile donors. In addition, the hemilabile donors can bind reversibly to Mn, but otherwise have minimal steric or electronic impact on the metal center. With this series of hemilabile donor pincer Mn complexes in hand, comparative studies of catalytic CO_2

hydrogenation were used to evaluate the role of these ligand alterations toward achieving improved first-row metal catalysis.

Catalytic CO_2 Hydrogenation to Formate

The performance of the Mn hydride complexes (**1-R**) for catalytic CO_2 hydrogenation to formate was initially investigated under conditions previously studied for the analog without the hemilabile substituent, **1-Me** (Table 1). In a typical experiment, 0.3 μmol of **1-R** was treated with 1000 psi of 1:1 H_2 and CO_2 at 80 °C in THF in the presence of 1,8-diazabicyclo[5.4.0]undec-7-ene (DBU) and lithium triflate (LiOTf). The DBU base improves the thermodynamics of the otherwise unfavorable hydrogenation of CO_2 to formic acid, and LiOTf acts as a Lewis acid co-catalyst to aid in formate release from Mn.[2a,8k,11e,12d] As observed for other first-row metal catalysts, the presence of LiOTf is essential to achieve high catalytic productivity (see SIV).[11e,12d] Catalyst **1-Me** was previously reported as the state-of-the-art Mn system with an aliphatic PNP ligand and in our hands achieves turnover numbers of 3,500 after 1h, 17,300 after 24h, and 19,200 after 72h with a maximum formate yield of 77% based on DBU (Entry 1). The TON after 1h is the primary

Table 1: Performance of different Mn catalysts in CO_2 hydrogenation to formate.[a]

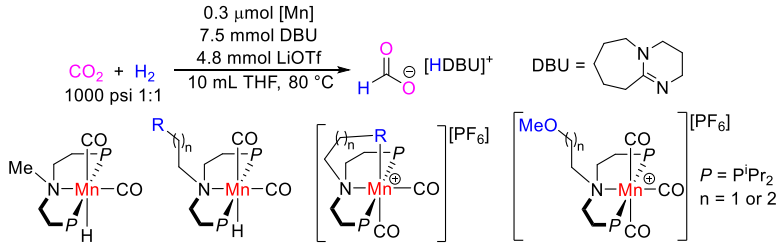

1-Me **1-R** **2-R** **3-R**

Entry	Compound	TON[b] (1h)	TON[b] (24h)	TON[b] (72h)	Yield[c] (%)
1	**1-Me**	3500 ± 200	17,300 ± 800	19,200 ± 1300	77
2	**1-^{2}OMe**	2000 ± 700	4800 ± 400	6900 ± 900	28
3	**1-P^{i}Pr$_2$**	800 ± 200	4000 ± 500	8600 ± 700	34
4	**1-NMe$_2$**	620 ± 20	9800 ± 200	15,100 ± 500	60
5	**1-^{3}OMe**	6100 ± 500	16,200 ± 500	25,100 ± 900	101
6	**2-^{2}OMe**	1000 ± 100	13,600 ± 700	21,700 ± 800	87
7	**2-^{3}OMe**	1400 ± 100	13,500 ± 500	18,800 ± 1100	75
8	**3-^{3}OMe**	670 ± 90	14,000 ± 1300	ND[d]	ND[d]

[a]Reaction conditions: 1000 psi of CO_2/H_2 (1:1), 0.3 μmol of catalyst in 10 mL of THF, 1.14 g DBU (7.6 mmol), 750 mg LiOTf (4.8 mmol) at 80 °C. [b]Formate product was quantified by ^{1}H NMR spectroscopy. Reported values are the average of at least two trials. [c]Reported yields are based on a 1:1 ratio of DBU:formate after 72h. Yields above 100% are possible as DBU can stabilize more than one formate ion via homoconjugation. [d]Not determined.

indicator of the rate of catalysis, as there is likely minimal catalyst decomposition at this early stage, thus this value provides an approximate TOF. The ~10% increase in TON after 24h shows that **1-Me** maintains some activity after 1 day, which is in stark contrast to the related Fe complex ($^{iPr}PN^{Me}P$)FeH(κ^1-BH_4)(CO) (**II**) which ceases activity after 3h under similar conditions.[21] Nevertheless, catalyst decomposition remains a major limitation for **1-Me**.

The introduction of the pendant arm in complexes of the type **1-R** has a profound and varied impact on catalytic CO_2 hydrogenation (Entries 2-5). TONs after 1h range from just 620 in the case of **1-NMe$_2$** to 6,100 for **1-^{3}OMe**, which is approximately 60% greater than for **1-Me**. Further, there is considerable variation in the TONs achieved after 72h. **1-^{2}OMe** gave a TON of only 6,900, corresponding to a 28% yield, while **1-^{3}OMe**, which contains only a single extra methylene group in the linker to the pendant donor, gave a TON of 25,100, corresponding to a yield of 101%. Yields over 100% based on DBU have been observed in previous systems and has been attributed to DBU stabilization of more than one formate ion via homoconjugation/homoassociation, an interaction between [HDBU]+ and formate through hydrogen bonds. This is again superior performance to **1-Me**. It is notable that the **1-R** catalysts with a pendant arm show a significant increase in TON between 24h and 72h, a feature not observed for **1-Me**. In the case of **1-P^{i}Pr$_2$**, formate production more than doubled over this period, while the minimum increase in TON was 30% for **1-^{2}OMe**. Entries 1-5 indicate that while the hemilabile substituent on the $^{iPr}PN^{R}P$ ligand has variable influences on the TOF and TON for CO_2 hydrogenation, the incorporation of the pendant arm consistently leads to improved catalyst lifetimes.

Commented [JW1]: Munshi JACS 2002, 124, 7963; Getty OM 2009, 28, 5466; Jeletic ACS Catal 2014, 4, 3755; Zhang Chem Sci 2015 6, 4291; Curley IC 2022, 61, 643

Commented [JW2]: Muller, Pure Appl Chem 1994, vol 66, 1077-1184, pp 1121. 10.1351/pac199466051077

Commented [WB3]: I suggest cutting this part out

One hypothesis for the improved lifetimes observed for complexes with pendant arms is that coordination of the hemilabile donor results in the formation of off-cycle species, similar to **2-R**, which can reversibly reenter the catalytic cycle. This may slow bimetallic catalyst decomposition by maintaining lower concentrations of coordinatively unsaturated Mn species in solution. To probe the role of species with the pendant arm bound in catalysis, we evaluated the catalytic performance of **2-^{2}OMe** and **2-^{3}OMe** (Entries 6 & 7). When **2-^{2}OMe** was used as a precatalyst, a lower TON was observed after 1h compared to **1-^{2}OMe**, but significantly increased turnovers after 24h and 72h. In fact, after 72h a yield of 87% was observed, which is superior to **1-Me**. These results conclusively demonstrate that **2-^{2}OMe** can enter the catalytic cycle and are consistent with it being an off-cycle resting state that protects the Mn center from deactivation but lowers initial TOF. **2-^{3}OMe** is also catalytically active but gives a lower TON than **1-^{3}OMe** at all time points

with the difference being most pronounced at 1h. These results suggest that **2-^{3}OMe** is not a significant resting state for **1-^{3}OMe**, although transient pendant arm binding could still aid in catalysis with **1-^{3}OMe** by inhibiting deactivation of the catalyst. However, the instability of **2-^{3}OMe** towards isolation complicates this analysis as at least 10% conversion of **2-^{3}OMe** to **3-^{3}OMe** occurs before conducting catalysis. Therefore, decomposition of **2-^{3}OMe** to **3-^{3}OMe** may also influence the relative catalytic performance (*vide infra*). Still, the different catalytic performances observed for **2-^{2}OMe** and **2-^{3}OMe** reinforce that even small changes to the pendant arm can have significant effects on catalysis and suggest that further optimization of the pendant arm could result in additional improvement.

In CO_2 hydrogenation using (^{iPr}PN^{Me}P)Fe(CO)H$_2$ (**II**), the Fe catalyst is proposed to undergo bimetallic decomposition involving the transfer of carbonyl ligands to generate catalytically-inactive species such as (^{iPr}PN^{Me}P)Fe(CO)$_2$ and [(^{iPr}PN^{Me}P)FeH(CO)$_2$]$^+$, along with free ligand and metallic Fe.[12d,16d] The observation of **3-^{3}OMe** as a contaminant in the synthesis of **2-^{3}OMe** suggests that Mn complexes undergo similar bimetallic decomposition. However, in contrast to the dicarbonyl Fe complexes, **3-^{3}OMe** is catalytically active for CO_2 hydrogenation (Entry 8). **3-^{3}OMe** produced significantly less formate after 1h compared to **1-^{3}OMe** but achieved only a slightly lower TON after 24h. This suggests that at least one CO ligand in **3-^{3}OMe** is labile, which allows access to an on-cycle species. Even though the formation of **3-^{3}OMe** in catalysis would likely require decay of a second equivalent of Mn complex (due to the need for another equivalent of CO), the fact that **3-^{3}OMe** is catalytically active is likely a significant advantage of using PNP-ligated Mn catalysts over related Fe systems.

Given that **1-^{3}OMe** achieved essentially full conversion after 72h under our standard conditions, we performed experiments at lower catalyst loading (Table 2). To achieve high yields at lower catalyst loading, increased temperature was required, as well as a change in the ratio of

Table 2: Optimization of **1-^{3}OMe** in CO_2 hydrogenation to formate.[a]

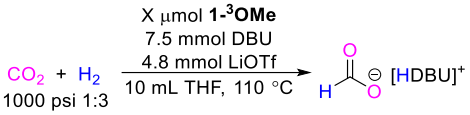

Entry	[Mn] (μmol)	TON[b] (1h)	TON[b] (72h)	Yield[c] (%)
1	0.030		242,000 ± 22,000	97
2	0.015	158,000 ± 32,000	443,000 ± 48,000	89
3	0.003		838,000 ± 69,000	34
4[d]	0.015		482,000	97
5[e]	0.015		496,000	99

[a]Reaction conditions: 1000 psi of CO_2/H_2 (1:3), X μmol of **1-^{3}OMe** in 10 mL of THF, 1.14 g DBU (7.6 mmol), 750 mg LiOTf (4.8 mmol) at 110 ºC. [b]Formate product was quantified by ^{1}H NMR spectroscopy. Values with esd are the average of at least two trials. [c]Reported yields are based on a 1:1 ratio of DBU:formate after 72h. [d]With Hg drop added. [e]With 0.0075 μmol PMe_3 added.

the CO_2 to H_2 feedstock gas from 1:1 to 1:3 (see SIV for optimization). At 0.030 and 0.015 μmol loading of Mn (Entries 1 and 2), the yields of formate were 97 and 89%, respectively. This corresponds to TONs of 242,000 and 443,000, respectively. We were able to achieve a maximum TON of 838,000 at 0.003 μmol Mn loading, which equates to 34% yield (Entry 3). Further experiments were performed at 0.015 μmol loading of Mn because this was the lowest loading at which high conversion was obtained. After 1h, a TOF of 158,000 was achieved, demonstrating that **1-^{3}OMe** has exceptional activity, as well as productivity (Entry 3). The higher TOF at lower catalyst loading is consistent with the catalyst decomposing via a process that is greater than first order in [Mn]. Two experiments were performed to provide evidence for homogeneous catalysis. When a reaction was performed with a drop of Hg, the TON after 72h is within error as the TON with no Hg present (Entry 4). Similarly, a reaction performed with a sub-stoichiometric amount of exogeneous PMe_3 did not significantly impact the TON (Entry 5). Finally, at 0.015 μmol Mn loading, the control complex **1-Me** containing a pincer ligand without a pendant arm gave only 166,000 turnovers after 72h (see SIV), again demonstrating the significant beneficial impact of the pendant arm on catalytic performance.

The TON observed for **1-^{3}OMe** makes it the most productive well-defined first-row transition metal catalyst for CO_2 hydrogenation to formate, notwithstanding the challenges associated with

comparing catalysts under different conditions. For comparison, a maximum TON of 31,600 was reported for a Mn complex supported by a pyridine-based PNNNP ligand (**III**, Figure 1b) in THF/H_2O at 100 °C using DBU and LiOTf as an additive at 0.2 μmol catalyst loading[12] and a related Mn complex supported by a more complicated triazene-based PNNNP ligand (**IV**, Figure 1b) achieves a TON of 230,000 in THF/H_2O at 115 °C using lysine as a base/additive at 0.02 μmol loading.[13] The only reported first-row transition metal system that gives a higher TON than **1-^{3}OMe** is formed by *in situ* mixing of a Ni salt with a tridentate phosphine ligand and the nature of the active catalyst is unclear.[14d] In fact, **1-^{3}OMe** is more productive than all but one precious metal system for CO_2 hydrogenation to formate (see SI for a comprehensive list) and is unusual because it gives both high yields and TONs. The TOF of **1-^{3}OMe** is also exceptional compared to other homogeneous systems and surpasses even the best precious metal systems. Further, we suggest that the strategy of incorporating an additional pendant donor into a pincer ligand could increase the TON of many of the catalysts featuring pincer ligands where bimolecular catalyst decomposition is proposed.[16d] Hence, **1-^{3}OMe** represents not only a highly productive catalyst but also provides proof-of-principle for a potentially general approach for designing improved pincer-ligated catalysts.

Mechanistic Studies of CO_2 Hydrogenation to Formate

The exceptional performance of **1-^{3}OMe** motivated additional examination of the mechanism for CO_2 hydrogenation and the features that most impact catalyst productivity. More detailed mechanistic knowledge could also provide understanding of the trends in CO_2 hydrogenation observed for catalysts supported with pincer ligands containing different pendant arms (Table 1). Based on previous studies using **1-Me**,[11e] we propose that the first step in catalysis with **1-^{3}OMe** is CO_2 insertion into the Mn hydride to form a formate complex. Consistent with this hypothesis, exposure of **1-^{3}OMe** to 1 atm of CO_2 in THF-d_8 leads to the quantitative formation of the formate complex (^{iPr}PN^{3OMe}P)Mn(CO)$_2${OC(O)H} within 15 minutes at ambient temperature (Figure 6). Similar reactivity was observed with **1-^{2}OMe**. Under ambient conditions **1-^{3}OMe** does not react with base or H_2 individually (see SV), providing further support to a first step involving CO_2 insertion. (^{iPr}PN^{3OMe}P)Mn(CO)$_2${OC(O)H} could not be isolated as decarboxylation occurs upon exposure to vacuum to regenerate **1-^{3}OMe**. This near thermoneutrality of CO_2 insertion is likely a benefit in catalysis as it avoids the formation of an overly thermodynamically stable formate complex, which is less likely to undergo further reactions. It is notable that

(^{iPr}PN^{Me}P)Mn(CO)$_2${OC(O)H}, which lacks a hemilabile donor, is isolable,[11e] suggesting that CO_2 insertion into **1-Me** is more thermodynamically favorable. This decreased thermodynamic favorability of CO_2 insertion into **1-^{3}OMe** likely contributes to the increase in TOF observed for **1-^{3}OMe** compared to **1-Me**.

In THF solution at ambient temperature under a CO_2 atmosphere, (^{iPr}PN^{3OMe}P)Mn(CO)$_2$-{OC(O)H} is stable for days. The addition of $LiPF_6$ produces **2-^{3}OMe** and a precipitate which is likely lithium formate (Figure 6). In contrast, there is no reaction when (^{iPr}PN^{Me}P)Mn(CO)$_2$-

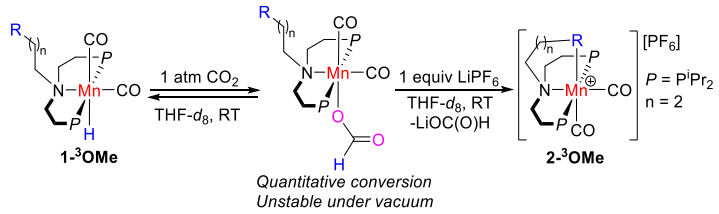

Figure 6: Stoichiometric CO_2 insertion and formate loss from **1-^{3}OMe**.

{OC(O)H} is exposed to $LiPF_6$ (see SVc), demonstrating that the pendant arm can facilitate unique reactivity and possibly enhance the influence of Lewis acidic additives. While **2-^{3}OMe** does not react with DBU or 1 atm of H_2 individually, addition of 1 atm of H_2 and DBU to **2-^{3}OMe** generates the *syn*-isomer of **1-^{3}OMe** immediately at room temperature (Figure 7). In the *syn*-isomer, which is not observed after crystallization of **1-^{3}OMe** and is therefore thermodynamically disfavored, the hydride is on the same face of the Mn as the pendant arm. This suggests that when exposed to H_2, **2-^{3}OMe** is in equilibrium with the *syn*-isomer of a Mn dihydrogen complex.[16d] The equilibrium favors **2-^{3}OMe**, but addition of base results in deprotonation of the bound H_2 and the formation of *syn*-**1-^{3}OMe**, which isomerizes over time to *anti*-**1-^{3}OMe** (see SVd). In comparison, the addition of 1 atm of H_2 and DBU to **2-^{2}OMe** formed *syn*-**1-^{2}OMe**, but the reaction took significantly longer with only ~10% conversion after 6 hours. This suggests that the equilibrium between **2-^{2}OMe**, H_2, and a molecular H_2 complex favors **2-^{2}OMe** more so than **2-^{3}OMe**, demonstrating that linker length and resulting chelating ring size can impact elementary steps relevant to catalysis. These

observations suggest a pathway for **2-^{2}OMe** and **2-^{3}OMe** to enter the catalytic cycle and agree with the higher TOF in catalysis using **2-^{3}OMe** as a precatalyst compared to **2-^{2}OMe**.

To gain insight into the speciation of Mn during catalysis, NMR studies were performed under modified catalytic conditions. Upon addition of 1 atmosphere 1:1 CO_2/H_2, 30 equiv DBU, and 3 equiv LiOTf to a solution of **1-^{3}OMe** in THF-d_8 at 60 °C, immediate conversion to the formate species (^{iPr}PN^{3OMe}P)Mn(CO)$_2${OC(O)H} was observed. After 1h, (^{iPr}PN^{3OMe}P)Mn(CO)$_2$-{OC(O)H} was observed as the major species in the ^{31}P NMR spectrum, along with **3-^{3}OMe** and free ligand. The gradual growth of [HDBU$^+$][HCOO$^-$] was observed in the ^{1}H NMR spectrum along with a white precipitate presumed to contain formate salts of [HDBU$^+$] and [Li$^+$], consistent with catalysis occurring (see SVf). Similar results were observed when we monitored catalyst speciation using **2-^{3}OMe** as the precatalyst, except the quantity of **3-^{3}OMe** was significantly higher, perhaps due to the instability of **2-^{3}OMe**. Finally, in a reaction using **3-^{3}OMe** as the precatalyst, (^{iPr}PN^{3OMe}P)Mn(CO)$_2${OC(O)H} and **3-^{3}OMe** were observed, providing further support that one CO ligand in **3-^{3}OMe** is labile. Taken together these results demonstrate that (^{iPr}PN^{3OMe}P)Mn(CO)$_2${OC(O)H} is the major catalyst resting state using **1-^{3}OMe** or **2-^{3}OMe**

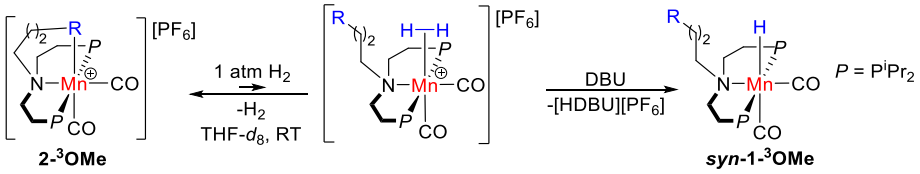

Figure 7: Formation of **1-^{3}OMe** from **2-^{3}OMe** under catalytically relevant conditions.

under our modified conditions. This suggests that even though the pendant arm may be able to slow catalyst decomposition by inhibiting the formation of the coordinatively unsaturated species via transient binding, the pendant arm does not bind sufficiently tightly to inhibit catalysis by shifting the Mn to an off-cycle resting state. Presumably, this is a major reason for the exceptional performance of **1-^{3}OMe**. Further, the fact that similar catalyst speciation is observed starting with **1-^{3}OMe** or **2-^{3}OMe** is consistent with their comparable catalytic performance at 24h, especially when the instability of **2-^{3}OMe** is considered.

Several stoichiometric experiments suggest that the binding of the two-carbon linked pendant arm in **2-^{2}OMe** is more favored than binding of the three-carbon linked pendant arm in **2-^{3}OMe** (*vide supra*). When catalyst speciation was monitored using **1-^{2}OMe** or **2-^{2}OMe** as (pre)catalysts in trials under the modified catalytic conditions, both the formate complex and **2-^{2}OMe** were

observed at 1h (see SVf). This indicates that some of the Mn is in an off-cycle form with the pendant arm coordinated, which could explain the lower catalytic performance of **1-^{2}OMe** compared to **1-^{3}OMe**. Further, the improved catalytic performance of **2-^{2}OMe** compared to **1-^{2}OMe** at extended reaction times is consistent with a bimetallic catalyst decomposition pathway, as the concentration of coordinatively saturated species in solution is lower since a portion of Mn is sequestered as **2-^{2}OMe**.

Our proposed mechanism for **1-^{2}OMe** and **1-^{3}OMe** catalyzed CO_2 hydrogenation to formate is shown in Figure 8. Initially, CO_2 inserts into the Mn–H bond in **1-R** to generate a Mn formate complex. Subsequently, formate displacement assisted by Li^+ from (^{iPr}PN^{R}P)Mn(CO)$_2${OC(O)H} forms a Mn molecular hydrogen complex. The molecular hydrogen complex is in equilibrium with an off-cycle species **2-R**, where the pendant arm displaces the bound H_2 molecule. This equilibrium is highly dependent on the identity of the pendant arm, with the two-carbon linker in **1-^{2}OMe** exhibiting a greater preference for pendant arm coordination than the three-carbon linker in **1-^{3}OMe**. Finally, deprotonation of the molecular hydrogen complex with DBU regenerates **1-R** to close the cycle. The formate displacement step is likely the turnover limiting step on the cycle, although during the reaction some Mn can accumulate in the form of the off-cycle species **2-R** in cases where pendant arm binding is thermodynamically favorable. Both (^{iPr}PN^{R}P)Mn{OC(O)H}(CO)$_2$ and **2-R** were observed as the resting states during catalytic trials monitored by NMR spectroscopy. This analysis is also supported by DFT calculations (vide infra). Formate displacement is also proposed to be the turnover limiting step in many other PNP-supported catalysts. It is notable that the cycle does not require any steps involving metal-ligand cooperativity, which has previously been proposed as crucial for CO_2 hydrogenation.[5b,30]

Commented [JW4]: Include refs here

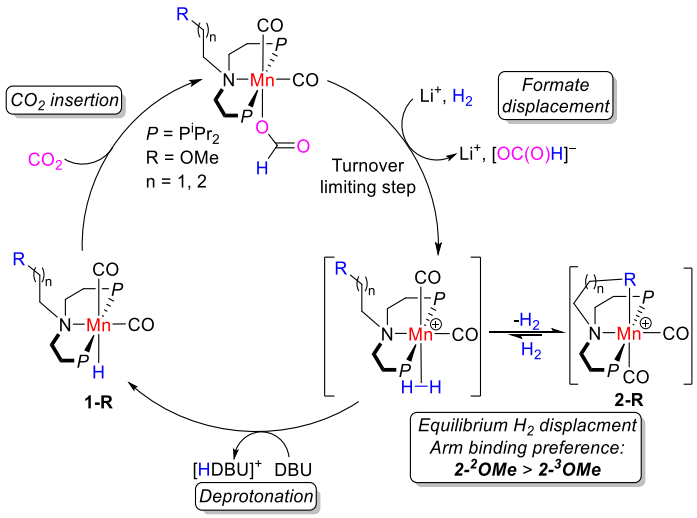

Figure 8: Proposed mechanism for CO_2 hydrogenation using **1-^{2}OMe** and **1-^{3}OMe**. Only the thermodynamically preferred isomer is shown for all species.

The major difference between the mechanism proposed for ligands with a pendant arm compared to that previously proposed for **1-Me** is the potential formation of the off-cycle species, **2-R**, with the pendant arm bound.[11e] Given that decomposition of the catalyst likely occurs at least partially through the formation of coordinatively unsaturated species of the type $[(\kappa^3\text{-}^{iPr}PN^RP)Mn(CO)_2)]^+$, the proposed mechanism explains the increased catalyst longevity observed for systems containing an additional donor on the pincer ligand. The ability of the pendant arm to bind reduces the concentration of $[(\kappa^3\text{-}^{iPr}PN^RP)Mn(CO)_2)]^+$, resulting in slower deactivation. DFT calculations show that the energy required to access $[(\kappa^3\text{-}^{iPr}PN^RP)Mn(CO)_2)]^+$ from $[(^{iPr}PN^{Me}P)Mn(CO)_2(H_2)]^+$ by loss of H_2 is only 1.8 kcal mol^{-1} uphill. In contrast, decoordination of the pendant arm in **2-^{3}OMe** is 7.0 kcal mol^{-1} uphill confirming that it will be harder to access a coordinatively unsaturated complex with the $^{iPr}PN^{3OMe}P$ ligand (see SVI).

The mechanism shown in Figure 8 assists in rationalizing the trends in catalytic CO_2 hydrogenation performance based on the identity of the hemilabile substituent of the pincer ligand (Table 1, Entries 1-5). At extended reaction times (24h) the performance of the Mn hydride catalysts **1-R** should be influenced by two factors: (i) the relative equilibrium between a complex with a pendant arm bound in **2-R** and a Mn molecular hydrogen complex, and (ii) the amount of catalyst that has decomposed. This assumes minimal involvement of the pendant arm in on-cycle

steps in catalysis. Factor (i) partially controls the amount of Mn available to produce formate and the amount of Mn sequestered off-cycle. DFT calculations were used to compare the thermodynamic energy required to convert **2-R** and H_2 to the on-cycle Mn molecular hydrogen complex $[(^{iPr}PN^{R}P)Mn(CO)_2(H_2)]^+$, as either the *syn* or *anti*-isomers (Table 3, SVI). It is most challenging to displace the pendant donor for **2-^{2}OMe** and **2-NMe$_2$**. This is consistent with the poor relative performance of these catalysts after 24h as the pendant arm coordinated species cannot readily reenter the catalytic cycle. However, the excellent catalytic performance of **2-^{2}OMe** after 24h indicates that a slower rate of formate production due to a lower concentration of on-cycle Mn species may be balanced over time by a reduction in catalyst deactivation. While complexes of the type **1-R** are relatively stable in solution, heating a C_6D_6 solution of $(^{iPr}PN^{R}P)Mn(CO)_2\{OC(O)H\}$ (R = OMe, CH_2OMe) in an NMR tube at 55 °C showed the growth of an unknown species at 50 ppm (see SVg). This observation along with the comparative catalytic trials between **1-^{2}OMe** and **2-^{2}OMe** suggest that there is a decomposition pathway that does not involve the formation of **2-^{2}OMe**. Over extended reaction times, the limitations in the catalytic performance of **1-^{2}OMe** appear more dependent on its rate of decomposition while on-cycle (factor (ii)) rather than on the relatively strong binding of the arm compared to H_2 coordination (factor (i)).

For **2-^{3}OMe**, displacement of the pendant arm by H_2 is calculated to be slightly easier than for **2-^{2}OMe** and **2-NMe$_2$**, which provides some rationale for its excellent catalytic performance. Presumably pendant arm displacement is easier in **2-^{3}OMe** because the six-membered ring formed from pendant arm binding is less favored than the five-membered rings formed from pendant arm

Table 3: Calculated energy for conversion of arm-bound species to molecular H_2 complex.

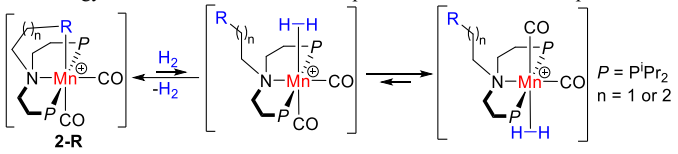

Entry	Compound	Calculated ΔG (kcal/mol) for arm displacement by H_2[a]	Calculated ΔG (kcal/mol) for *syn* to *anti* isomerization
1	**2-^{2}OMe**	5.0	0.1
2	**2-P^{i}Pr$_2$**	−0.3	0.3
3	**2-NMe$_2$**	3.6	−0.4
4	**2-^{3}OMe**	1.3	−2.2

[a]Calculations were performed with the Gaussian16 software package using the M06l functional, LanL2DZ basis set for Mn, 6-31+G** for other atoms, and the CPCM solvent model (THF). See SVI for details. The energy of free H_2 was included to balance stoichiometry.

binding in **2-^{2}OMe** and **2-NMe$_2$**. Notably, formation of the *anti*-isomer of [(^{iPr}PN^{3OMe}P)Mn(CO)$_2$(H$_2$)]$^+$ from **2-R** and H_2 is calculated to be thermodynamically downhill. However, presumably there is no direct pathway for the formation of *anti*-[(^{iPr}PN^{3OMe}P)Mn(CO)$_2$(H$_2$)]$^+$ from **2-^{3}OMe** and H_2, as we see no reaction between **2-^{3}OMe** and H_2 experimentally. Nevertheless, these results agree with **2-^{3}OMe** not being the resting state in catalysis with **1-^{3}OMe**. For **2-P^{i}Pr$_2$**, displacement of the arm by H_2 is calculated to be slightly thermodynamically downhill which implies that the relatively poor catalytic performance of **1-P^{i}Pr$_2$** is not related to strong binding of the pendant arm. Steric factors likely make the binding of the extra P^{i}Pr$_2$ group in ^{iPr}PN^{PiPr2}P unfavorable despite the expected stronger σ-donation from the phosphine. Indeed, when calculations were performed using the hypothetical ligand ^{iPr}PN^{PMe2}P, which features a pendant phosphine donor bearing methyl substituents, coordination of the pendant arm was highly favorable (see SVI). The presence of three phosphine donors in ^{iPr}PN^{PiPr2}P may also result in alternative speciation of the catalyst. For example, it is possible that the ligand can bind through three P donors without the central N donating, which has been reported in Fe complexes.[20e,31] Due to the poor overall performance of **1-P^{i}Pr$_2$**, this was not explored further.

One aspect of the catalytic performance of our different systems that is challenging to fully rationalize is the initial activity after 1h (Table 1). At this early reaction time, catalyst decomposition of **1-R** is likely less significant and the initial activity is a combination of two factors: (i) the ability of formate in (^{iPr}PN^{R}P)Mn(CO)$_2${OC(O)H} to be displaced from the Mn center by H_2, and (ii) the tendency of the catalyst to form the off-cycle species **2-R**. Comparing the calculated thermodynamic energy for the conversion of (^{iPr}PN^{R}P)Mn(CO)$_2${OC(O)H} to [(^{iPr}PN^{R}P)Mn(CO)$_2$(H$_2$)]$^+$ provides an estimate of the difficulty for formate release (Table 4). This process is likely irreversible as formate salts precipitate out of solution. The data shows that the energy required for formate displacement is similar for all complexes except for (^{iPr}PN^{3OMe}P)Mn(CO)$_2${OC(O)H}. In this case, formate displacement is significantly easier (~2 kcal mol^{-1}), which may explain the high initial activity of **1-^{3}OMe**. It is unclear exactly why formate displacement is easier for (^{iPr}PN^{3OMe}P)Mn(CO)$_2${OC(O)H}. In contrast, given that the energy required for formate displacement from all other complexes is calculated to be similar,

Table 4: Calculated energy for conversion of formate complex to molecular hydrogen complex.

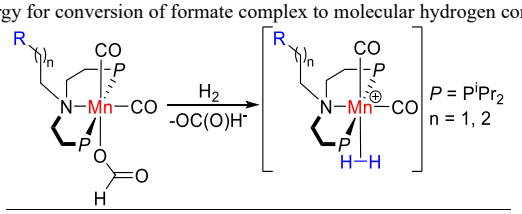

Entry	Ligand	Calculated ΔG (kcal/mol) for H_2 displacement of formate[a]
1	^{iPr}PN^{Me}P	23.3
2	^{iPr}PN^{2OMe}P	23.4
3	^{iPr}PN^{PiPr2}P	23.6
4	^{iPr}PN^{NMe2}P	23.7
5	^{iPr}PN^{3OMe}P	21.4

[a]Calculations were performed with the Gaussian16 software package using the M06l functional, LanL2DZ basis set for Mn, 6-31+G** for other atoms, and the CPCM solvent model (THF). See SVI for details. The energy of free H_2 and formate were included to balance stoichiometry. Modelling formate in solution is challenging and hence the absolute energies presented here are not significant, but the trends are likely important.

thermodynamic factors do not explain the large differences in initial activity for these systems. Further work is required to understand this phenomenon. In general, the complexity of the catalytic systems makes fully rationalizing the observed trends with different ligands difficult but our relatively simple analysis explains many of the key observations. To completely model the observed catalytic performance detailed knowledge of all the catalytic intermediates and decomposition pathways, as well as relative rates is required. This information is challenging to obtain experimentally but will be explored using kinetic simulations based on DFT calculations in future work.

Conclusions

In this work, we prepared ^{iPr}PN^{R}P pincer ligands with an additional hemilabile pendant ether, amine, or phosphine donor. These ligands were used to support Mn hydride catalysts for the hydrogenation of CO_2 to formate. Comparative catalytic studies, combined with mechanistic studies, reveal that the hemilabile donor identity strongly impacts catalyst performance. All complexes containing a pincer ligand with an additional hemilabile donor display improved catalytic lifetimes in comparison to a control complex containing a more widely used pincer ligand without a pendant donor. The improved catalytic performance is likely due to the hemilabile coordination which inhibits catalyst decomposition routes that occur via coordinatively unsaturated species. However, the strength of binding of the hemilabile ligand is crucial in

determining catalyst activity and productivity. If the hemilabile ligand binds too tightly, as is the case for $^{iPr}PN^{2OMe}P$ and $^{iPr}PN^{NMe2}P$, the catalyst resting state is partially an off-cycle species with the arm bound, and this leads to a decrease in catalytic activity. In the case of the $^{iPr}PN^{3OMe}P$ ligand, arm binding is less favored and the catalyst resting state remains an on-cycle species, though transient arm binding likely still inhibits catalyst decomposition. Consequently, ($^{iPr}PN^{3OMe}P$)$Mn(CO)_2H$ is one of the most active and productive catalysts reported for CO_2 hydrogenation to formate. It gives a TOF of up to 158,000 h^{-1} and a TON of up to 838,000, which are comparable with even the best precious metal catalysts.

Overall, our work demonstrates that the incorporation of an additional hemilabile arm on pincer ligands can significantly improve catalytic performance. We expect that this general strategy could apply to a plethora of other pincer ligands, for instance PNP ligands with a central pyridine donor, and to reactions beyond CO_2 hydrogenation. For example, improved catalytic performance will likely be observed in related reactions such as ester and amide formation and dehydrogenation reactions, which proceed via similar mechanisms. The key is to control the strength of the binding of the additional donor to facilitate catalyst stabilization, without creating an off-cycle resting state. Further work in our laboratories will focus on applying the use of catalysts containing pincer ligands with additional hemilabile donors to other reactions.

Methods

Synthesis of 1-^{3}OMe. In a 4 dram vial, ($^{iPr}PN^{3OMe}P$)$Mn(CO)_2Br$ (98 mg, 0.17 mmol) was dissolved in THF (5 mL) to form a yellow solution. $NaBH_4$ (20 mg, 0.53 mmol) was added along with EtOH (5 mL). Gas evolution was observed. The reaction was stirred overnight then filtered and dried under vacuum. The product was extracted into hexane (20 mL), the solution was filtered, then dried under vacuum to afford yellow solids of **1-^{3}OMe** as predominantly the *anti*-isomer (72 mg, 86%). Yellow crystals of the *anti*-isomer suitable for X-ray diffraction were grown from a concentrated Et_2O solution at -35 °C.

Representative Procedure for CO_2 Hydrogenation to Formate. In a glovebox under a nitrogen atmosphere, a glass liner suitable for a 50 mL Parr reactor base was charged with LiOTf (750 mg, 4.8 mmol), DBU (1.14 g, 7.5 mmol), 10 mL of ketyl-dried THF, and Mn catalyst as a stock solution in ketyl-dried THF (ca. 0.01 μM, 0.3 μmol). The glass liner was placed into the Parr reactor base, the ring collar was assembled, and the vessel was sealed. The reactor was removed from the glovebox and pressurized sequentially with 500 psi of CO_2 followed by 500 psi of H_2 at

ambient temperature. Over the course of 10 minutes, the reactor was heated to 80 °C and mechanically stirred for the desired length of time. The reaction was stopped by removing the reactor from the heating mantle and cooling for 30 minutes in an ice bath. The reactor was then vented and the reaction solution and solid residue was transferred to a 100 mL round-bottomed flask, using H_2O or D_2O to dissolve the solid products. Using 100 µL of DMF as an internal standard, the formate product was quantified by ^1H NMR spectroscopy.

Further details regarding the methods can be found in the supplemental information.

Resource Availability

Lead contact

Further information and requests for resources should be directed to and will be fulfilled by the lead contact, Nilay Hazari (nilay.hazari@yale.edu).

Materials Availability

Detailed information about the preparation and characterization of compounds is provided in the supplemental information.

Data and Code availability

Crystallographic data have been deposited in the Cambridge Crystallographic Data Center (CCDC) with accession numbers 2480429-2480432 & 2480434-2480438. These data can be obtained free of charge from the CCDC at https://www.ccdc.cam.ac.uk/structures/.

Acknowledgements

N.H. and W.H.B. acknowledge support from the U.S. Department of Energy, Office of Science, Basic Energy Sciences, Catalysis Science Program, under Award DE-SC0018222. All computational work was supported by the facilities and staff of the Yale University Faculty of Arts and Sciences High Performance Computing Center. This research made use of the Chemical and Biophysical Instrumentation Center at Yale University. We thank Dr. Fabian Menges for assistance with mass spectrometry and Dr. Tanya Townsend for preliminary studies towards the synthesis of pincer ligands with pendant arms.

Author Contributions

J.C.W. and K.B.V. synthesized and characterized the Mn complexes. J.C.W. and N.P. synthesized and characterized the PNP ligands. K.B.V. performed hydrogenation experiments. J.C.W. and

K.B.V. performed mechanistic studies. J.C.W. and B.Q.M. collected and analyzed the diffraction data. J.C.W. and N.H. wrote the first draft of the manuscript. J.C.W., K.B.V., W.H.B., and N.H. revised the text. W.H.B. and N.H. supervised the work and obtained funding.

Declaration of Interests

The authors declare no competing interests.

Supplemental Information

Document S1. Tables S1-S35, Figures S1-S146, detailed experimental procedures, characterization data, details of additional experiments, NMR and IR spectra, computational details, X-ray crystallographic information, and supplemental references.

References

Commented [JW5]: We need to make each reference number its own paper. We cannot have a,b,c etc. and we cannot have footnotes in the references

1. (a) Klankermayer, J.; Wesselbaum, S.; Beydoun, K.; Leitner, W. Selective Catalytic Synthesis Using the Combination of Carbon Dioxide and Hydrogen: Catalytic Chess at the Interface of Energy and Chemistry. *Angew. Chem. Int. Ed.* **2016**, *55*, 7296; (b) Artz, J.; Müller, T. E.; Thenert, K.; Kleinekorte, J.; Meys, R.; Sternberg, A.; Bardow, A.; Leitner, W. Sustainable Conversion of Carbon Dioxide: An Integrated Review of Catalysis and Life Cycle Assessment. *Chem. Rev.* **2018**, *118*, 434; (c) Burkart, M. D.; Hazari, N.; Tway, C. L.; Zeitler, E. L. Opportunities and Challenges for Catalysis in Carbon Dioxide Utilization. *ACS Catal.* **2019**, *9*, 7937; (d) Hepburn, C.; Adlen, E.; Beddington, J.; Carter, E. A.; Fuss, S.; Mac Dowell, N.; Minx, J. C.; Smith, P.; Williams, C. K. The Technological and Economic Prospects for CO_2 Utilization and Removal. *Nature* **2019**, *575*, 87; (e) Gao, W.; Liang, S.; Wang, R.; Jiang, Q.; Zhang, Y.; Zheng, Q.; Xie, B.; Toe, C. Y.; Zhu, X.; Wang, J.; Huang, L.; Gao, Y.; Wang, Z.; Jo, C.; Wang, Q.; Wang, L.; Liu, Y.; Louis, B.; Scott, J.; Roger, A.-C. C.; Amal, R.; He, H.; Park, S.-E. E. Industrial Carbon Dioxide Capture and Utilization: State of the Art and Future Challenges. *Chem. Soc. Rev.* **2020**, *49*, 8584.

2. (a) Wang, W.-H.; Himeda, Y.; Muckerman, J. T.; Manbeck, G. F.; Fujita, E. CO_2 Hydrogenation to Formate and Methanol as an Alternative to Photo- and Electrochemical CO_2 Reduction. *Chem. Rev.* **2015**, *115*, 12936; (b) Bernskoetter, W. H.; Hazari, N. Reversible Hydrogenation of Carbon Dioxide to Formic Acid and Methanol: Lewis Acid Enhancement of Base Metal Catalysts. *Acc. Chem. Res.* **2017**, *50*, 1049; (c) Sordakis, K.; Tang, C.; Vogt, L. K.; Junge, H.; Dyson, P. J.; Beller, M.; Laurenczy, G. Homogeneous Catalysis for Sustainable Hydrogen Storage in Formic Acid and Alcohols. *Chem. Rev.* **2018**, *118*, 372.

3. (a) Mellmann, D.; Sponholz, P.; Junge, H.; Beller, M. Formic Acid as a Hydrogen Storage Material-Development of Homogeneous Catalysts for Selective Hydrogen Release. *Chem. Soc. Rev.* **2016**, *45*, 3954; (b) Singh, A. K.; Singh, S.; Kumar, A. Hydrogen Energy Future with Formic Acid: A Renewable Chemical Hydrogen Storage System. *Catal. Sci. Technol.* **2016**, *6*, 12; (c) Eppinger, J.; Huang, K.-W. Formic Acid as a Hydrogen Energy Carrier. *ACS Energy Lett.* **2017**, *2*, 188; (d) Bulushev, D. A.; Ross, J. R. H. Towards Sustainable Production of Formic Acid. *ChemSusChem* **2018**, *11*, 821; (e) Kumar, A.; Daw, P.; Milstein, D. Homogeneous Catalysis for Sustainable Energy: Hydrogen and Methanol Economies, Fuels from Biomass, and Related Topics. *Chem. Rev.* **2022**, *122*, 385.

4. (a) Acar, C.; Dincer, I.; Naterer, G. F. Review of Photocatalytic Water-Splitting Methods for Sustainable Hydrogen Production. *Int. J. Energy Res.* **2016**, *40*, 1449; (b) Grigoriev, S. A.; Fateev, V. N.; Bessarabov, D. G.; Millet, P. Current Status, Research Trends, and Challenges in Water Electrolysis Science and Technology. *Int. J. Hydrogen Energy* **2020**, *45*, 26036; (c) Chatenet, M.; Pollet, B. G.; Dekel, D. R.; Dionigi, F.; Deseure, J.; Millet, P.; Braatz, R. D.; Bazant, M. Z.; Eikerling, M.; Staffell, I. Water Electrolysis: from Textbook Knowledge to the Latest Scientific Strategies and Industrial Developments. *Chem. Soc. Rev.* **2022**, *51*, 4583.

5. For selected leading references see: (a) Himeda, Y.; Onozawa-Komatsuzaki, N.; Sugihara, H.; Kasuga, K. Recyclable Catalyst for Conversion of Carbon Dioxide into Formate Attributable to an Oxyanion on the Catalyst Ligand. *J. Am. Chem. Soc.* **2005**, *127*, 13118; (b) Tanaka, R.; Yamashita, M.; Nozaki, K. Catalytic Hydrogenation of Carbon Dioxide Using Ir(III)-Pincer Complexes. *J. Am. Chem. Soc.* **2009**, *131*, 14168; (c) Azua, A.; Sanz, S.; Peris, E. Water-Soluble Ir^{III} N-Heterocyclic Carbene Based Catalysts for the Reduction of CO_2 to Formate by Transfer Hydrogenation and the Deuteration of Aryl Amines in Water. *Chem. Eur. J.* **2011**, *17*, 3963; (d) Schmeier, T. J.;

Dobereiner, G. E.; Crabtree, R. H.; Hazari, N. Secondary Coordination Sphere Interactions Facilitate the Insertion Step in an Iridium(III) CO_2 Reduction Catalyst. *J. Am. Chem. Soc.* **2011**, *133*, 9274; (e) Hull, J. F.; Himeda, Y.; Wang, W. H.; Hashiguchi, B.; Periana, R.; Szalda, D. J.; Muckerman, J. T.; Fujita, E. Reversible Hydrogen Storage Using CO_2 and a Proton-Switchable Iridium Catalyst in Aqueous Media Under Mild Temperatures and Pressures. *Nature Chem.* **2012**, *4*, 383; (f) Maenaka, Y.; Suenobu, T.; Fukuzumi, S. Catalytic Interconversion Between Hydrogen and Formic Acid at Ambient Temperature and Pressure. *Energy Environ. Sci.* **2012**, *5*, 7360.

6. For selected leading references see: (a) Tsai, J. C.; Nicholas, K. M. Rhodium-Catalyzed Hydrogenation of Carbon Dioxide to Formic Acid. *J. Am. Chem. Soc.* **1992**, *114*, 5117; (b) Gassner, F.; Leitner, W. Hydrogenation of Carbon Dioxide to Formic Acid Using Water-Soluble Rhodium Catalysts. *J. Chem. Soc., Chem. Commun.* **1993**, *49*, 1465; (c) Fornika, R.; Görls, H.; Seemann, B.; Leitner, W. Complexes [(P_2)Rh(hfacac)](P_2 = Bidentate Chelating Phosphane, hfacac = hexafluoroacetylacetonate) as Catalysts for CO_2 Hydrogenation: Correlations Between Solid State Structures, ^{103}Rh NMR Shifts and Catalytic Activities. *J. Chem. Soc., Chem. Commun.* **1995**, 1479; (d) Joo, F.; Laurenczy, G.; Nadasdi, L.; Elek, J. Homogeneous Hydrogenation of Aqueous Hydrogen Carbonate to Formate Under Exceedingly Mild Conditions—A Novel Possibility of Carbon Dioxide Activation. *Chem. Commun.* **1999**, 971; (e) Li, Y.-N.; He, L.-N.; Liu, A.-H.; Lang, X.-D.; Yang, Z.-Z.; Yu, B.; Luan, C.-R. In situ Hydrogenation of Captured CO_2 to Formate with Polyethyleneimine and Rh/Monophosphine System. *Green Chem.* **2013**, *15*, 2825.

7. For selected leading references see: (a) Inoue, Y.; Izumida, H.; Sasaki, Y.; Hasimoto, H. Catalytic Fixation of Carbon Dioxide to Formic Acid by Transition-Metal Complexes Under Mild Conditions. *Chem. Lett.* **1976**, *5*, 863; (b) Kudo, K.; Sugita, N.; Takezaki, Y. No Title. *Nihon Kagaku Kaishi* **1977**, 302; (c) Sakamoto, M.; Shimizu, I.; Yamamoto, A. Synthesis of the First Carbon Dioxide Coordinated Palladium(0) Complex, Pd(η^2-CO_2)$(PMePh_2)_2$. *Organometallics* **1994**, *13*, 407.

8. For selected leading references see: (a) Jessop, P. G.; Ikariya, T.; Noyori, R. Homogeneous Catalytic Hydrogenation of Supercritical Carbon Dioxide. *Nature* **1994**, *368*, 231; (b) Jessop, P. G.; Hsiao, Y.; Ikariya, T.; Noyori, R. Homogeneous Catalysis in Supercritical Fluids: Hydrogenation of Supercritical Carbon Dioxide to Formic Acid, Alkyl Formates, and Formamides. *J. Am. Chem. Soc.* **1996**, *118*, 344; (c) Gao, Y.; Kuncheria, J. K.; Jenkins, H. A.; Puddephatt, R. J.; Yap, G. P. A. The Interconversion of Formic Acid and Hydrogen/Carbon Dioxide Using a Binuclear Ruthenium Complex Catalyst. *J. Chem. Soc., Dalton Trans.* **2000**, *2*, 3212; (d) Laurenczy, G.; Joó, F.; Nádasdi, L. Formation and Characterization of Water-Soluble Hydrido-Ruthenium(II) Complexes of 1,3,5-Triaza-7-phosphaadamantane and Their Catalytic Activity in Hydrogenation of CO_2 and HCO_3^- in Aqueous Solution. *Inorg. Chem.* **2000**, *39*, 5083; (e) Munshi, P.; Main, A. D.; Linehan, J. C.; Tai, C.-C.; Jessop, P. G. Hydrogenation of Carbon Dioxide Catalyzed by Ruthenium Trimethylphosphine Complexes: The Accelerating Effect of Certain Alcohols and Amines. *J. Am. Chem. Soc.* **2002**, *124*, 7963; (f) Schaub, T.; Paciello, R. A. A Process for the Synthesis of Formic Acid by CO_2 Hydrogenation: Thermodynamic Aspects and the Role of CO. *Angew. Chem. Int. Ed.* **2011**, *50*, 7278; (g) Wesselbaum, S.; Hintermair, U.; Leitner, W. Continuous-Flow Hydrogenation of Carbon Dioxide to Pure Formic Acid using an Integrated $scCO_{-2}$ Process with Immobilized Catalyst and Base. *Angew. Chem. Int. Ed.* **2012**, *51*, 8585; (h) Filonenko, G. A.; Van Putten, R.; Schulpen, E. N.; Hensen, E. J. M.; Pidko, E. A. Highly Efficient Reversible Hydrogenation of Carbon Dioxide to Formates Using a Ruthenium PNP-Pincer Catalyst. *ChemCatChem* **2014**, *6*, 1526; (i) Moret, S.; Dyson, P. J.; Laurenczy, G. Direct Synthesis of Formic Acid From Carbon Dioxide by Hydrogenation in Acidic Media. *Nature Commun.* **2014**, *5*, 4017; (j) Kothandaraman, J.; Kar, S.; Sen, R.; Goeppert, A.; Olah, G. A.; Prakash, G. K. S. Efficient Reversible Hydrogen Carrier System Based on Amine Reforming of Methanol. *J. Am. Chem. Soc.* **2017**, *139*, 2549; (k) Curley, J. B.; Hert, C.; Bernskoetter, W. H.; Hazari, N.; Mercado, B. Q. Control of Catalyst Isomers Using an N-Phenyl-Substituted $RN(CH_2CH_2P^iPr_2)_2$ Pincer Ligand in CO_2 Hydrogenation and Formic Acid Dehydrogenation. *Inorg. Chem.* **2022**, *61*, 643.

9. (a) Alig, L.; Fritz, M.; Schneider, S. First-Row Transition Metal (De) Hydrogenation Catalysis Based on Functional Pincer Ligands. *Chem. Rev.* **2018**, *119*, 2681; (b) Mukherjee, A.; Milstein, D. Homogeneous Catalysis by Cobalt and Manganese Pincer Complexes. *ACS Catal.* **2018**, *8*, 11435; (c) Elsby, M. R.; Baker, R. T. Strategies and Mechanisms of Metal–Ligand Cooperativity in First-Row Transition Metal Complex Catalysts. *Chem. Soc. Rev.* **2020**, *49*, 8933; (d) Wen, J.; Wang, F.; Zhang, X. Asymmetric Hydrogenation Catalyzed by First-Row Transition Metal Complexes. *Chem. Soc. Rev.* **2021**, *50*, 3211; (e) Singh, T.; Jalwal, S.; Chakraborty, S. Homogeneous First-Row Transition-Metal-Catalyzed Carbon Dioxide Hydrogenation to Formic Acid/Formate, and Methanol. *Asian J. Org. Chem.* **2022**, *11*.

10. (a) Darensbourg, D. J.; Ovalles, C. Anionic Group 6B Metal Carbonyls as Homogeneous Catalysts for Carbon Dioxide/Hydrogen Activation. The Production of Alkyl Formates. *J. Am. Chem. Soc.* **1984**, *106*, 3750; (b) Jing, Y.; Ye, Z.; Su, J.; Feng, Y.; Qu, L.-B.; Liu, Y.; Ke, Z. The Potential of d^6 Non-Noble Metal NHC Catalysts for Carbon Dioxide Hydrogenation: Group and Row Effects. *Catal. Sci. Technol.* **2020**, *10*, 5443; (c) Singh, T.; Gutal, A.; Regina, A.; Banerjee, A.; Paranjothy, M.; Chakraborty, S. Bench-Stable Low-Valent Chromium Catalysts for Hydrogenation of CO_2, Bicarbonate, and Inorganic Carbonates to Formate. *ACS Catal.* **2024**, *14*, 14958.

11. For selected leading references see: (a) Bertini, F.; Glatz, M.; Gorgas, N.; Stöger, B.; Peruzzini, M.; Veiros, L. F.; Kirchner, K.; Gonsalvi, L. Carbon Dioxide Hydrogenation Catalysed by Well-Defined Mn(I) PNP Pincer Hydride Complexes. *Chem. Sci.* **2017**, *8*, 5024; (b) Dubey, A.; Nencini, L.; Fayzullin, R. R.; Nervi, C.; Khusnutdinova, J. R. Bio-Inspired Mn(I) Complexes for the Hydrogenation of CO_2 to Formate and Formamide. *ACS Catal.* **2017**, *7*, 3864; (c) Kostera, S.; Weber, S.; Peruzzini, M.; Veiros, L. F.; Kirchner, K.; Gonsalvi, L. Carbon Dioxide Hydrogenation to Formate Catalyzed by a Bench-Stable, Non-Pincer-Type Mn(I) Alkylcarbonyl Complex. *Organometallics* **2021**, *40*, 1213; (d) Wei, D.; Sang, R.; Sponholz, P.; Junge, H.; Beller, M. Reversible Hydrogenation of Carbon Dioxide to Formic Acid using a Mn-Pincer Complex in the Presence of Lysine. *Nature Energ.* **2022**, *7*, 438; (e) Hert, C. M.; Curley, J. B.; Kelley, S. P.; Hazari, N.; Bernskoetter, W. H. Comparative CO_2 Hydrogenation Catalysis with MACHO-type Manganese Complexes. *Organometallics* **2022**, *41*, 3332; (f) Kostera, S.; Manca, G.; Gonsalvi, L. Carbon Dioxide Hydrogenation to Formate Catalyzed by a Neutral, Coordinatively Saturated Tris-Carbonyl Mn(I)-PNP Pincer-Type Complex. *Chem. Eur. J.* **2023**, *29*, e202302642; (g) Kostera, S.; Gonsalvi, L. Manganese(I) Catalyzed CO_2 Reduction Processes in Homogenous Phase. *ChemCatChem* **2024**, *16*, e202301391.

12. For selected leading references see: (a) Federsel, C.; Boddien, A.; Jackstell, R.; Jennerjahn, R.; Dyson, P. J.; Scopelliti, R.; Laurenczy, G.; Beller, M. A Well-Defined Iron Catalyst for the Reduction of Bicarbonates and Carbon Dioxide to Formates, Alkyl Formates, and Formamides. *Angew. Chem. Int. Ed.* **2010**, *49*, 9777; (b) Langer, R.; Diskin-Posner, Y.; Leitus, G.; Shimon, L. J. W.; Ben-David, Y.; Milstein, D. Low-Pressure Hydrogenation of Carbon Dioxide Catalyzed by an Iron Pincer Complex Exhibiting Noble Metal Activity. *Angew. Chem. Int. Ed.* **2011**, *50*, 9948; (c) Ziebart, C.; Federsel, C.; Anbarasan, P.; Jackstell, R.; Baumann, W.; Spannenberg, A.; Beller, M. Well-Defined Iron Catalyst for Improved Hydrogenation of Carbon Dioxide and Bicarbonate. *J. Am. Chem. Soc.* **2012**, *134*, 20701; (d) Zhang, Y.; MacIntosh, A. D.; Wong, J. L.; Bielinski, E. A.; Williard, P. G.; Mercado, B. Q.; Hazari, N.; Bernskoetter, W. H. Iron Catalyzed CO_2 Hydrogenation to Formate Enhanced by Lewis Acid Co-Catalysts. *Chem. Sci.* **2015**, *6*, 4291; (e) Rivada-Wheelaghan, O.; Dauth, A.; Leitus, G.; Diskin-Posner, Y.; Milstein, D. Synthesis and Reactivity of Iron Complexes with a New Pyrazine-Based Pincer Ligand, and Application in Catalytic Low-Pressure Hydrogenation of Carbon Dioxide. *Inorg. Chem.* **2015**, *54*, 4526; (f) Bertini, F.; Gorgas, N.; Stöger, B.; Peruzzini, M.; Veiros, L. F.; Kirchner, K.; Gonsalvi, L. Efficient and Mild Carbon Dioxide Hydrogenation to Formate Catalyzed by Fe(II) Hydrido Carbonyl Complexes Bearing 2,6-(Diaminopyridyl)diphosphine Pincer Ligands. *ACS Catal.* **2016**, *6*, 2889; (g) Kothandaraman, J.; Goeppert, A.; Czaun, M.; Olah, G. A.; Surya Prakash, G. K. CO_2 Capture by Amines in Aqueous Media and its Subsequent Conversion to Formate with Reusable Ruthenium and Iron Catalysts. *Green Chem.* **2016**, *18*, 5831; (h) Coufourier, S.; Gaignard Gaillard, Q.; Lohier, J.-F.; Poater, A.; Gaillard, S.; Renaud, J.-L. Hydrogenation of CO_2, Hydrogencarbonate, and Carbonate to Formate in Water using Phosphine Free Bifunctional Iron Complexes. *ACS Catal.* **2020**, *10*, 2108.

13. For selected leading references see: (a) Federsel, C.; Ziebart, C.; Jackstell, R.; Baumann, W.; Beller, M. Catalytic Hydrogenation of Carbon Dioxide and Bicarbonates with a Well-Defined Cobalt Dihydrogen Complex. *Chem. Eur. J.* **2012**, *18*, 72; (b) Jeletic, M. S.; Mock, M. T.; Appel, A. M.; Linehan, J. C. A Cobalt-Based Catalyst for the Hydrogenation of CO_2 Under Ambient Conditions. *J. Am. Chem. Soc.* **2013**, *135*, 11533; (c) Badiei, Y. M.; Wang, W.-H.; Hull, J. F.; Szalda, D. J.; Muckerman, J. T.; Himeda, Y.; Fujita, E. Cp*Co(III) Catalysts with Proton-Responsive Ligands for Carbon Dioxide Hydrogenation in Aqueous Media. *Inorg. Chem.* **2013**, *52*, 12576; (d) Spentzos, A. Z.; Barnes, C. L.; Bernskoetter, W. H. Effective Pincer Cobalt Precatalysts for Lewis Acid Assisted CO_2 Hydrogenation. *Inorg. Chem.* **2016**, *55*, 8225; (e) Burgess, S. A.; Grubel, K.; Appel, A. M.; Wiedner, E. S.; Linehan, J. C. Hydrogenation of CO_2 at Room Temperature and Low Pressure with a Cobalt Tetraphosphine Catalyst. *Inorg. Chem.* **2017**, *56*, 8580; (f) Vollmer, M. V.; Ye, J.; Linehan, J. C.; Graziano, B. J.; Preston, A.; Wiedner, E. S.; Lu, C. C. Cobalt-Group 13 Complexes Catalyze CO_2 Hydrogenation via a Co(−I)/Co(I) Redox Cycle. *ACS Catal.* **2020**, *10*, 2459.

14. For selected leading references see: (a) Tai, C.-C.; Chang, T.; Roller, B.; Jessop, P. G. High-Pressure Combinatorial Screening of Homogeneous Catalysts: Hydrogenation of Carbon Dioxide. *Inorg. Chem.* **2003**, *42*, 7340; (b) Burgess, S. A.; Kendall, A. J.; Tyler, D. R.; Linehan, J. C.; Appel, A. M. Hydrogenation of CO_2 in Water Using a Bis(diphosphine) Ni–H Complex. *ACS Catal.* **2017**, *7*, 3089; (c) Cammarota, R. C.; Vollmer, M. V.; Xie, J.; Ye, J.; Linehan, J. C.; Burgess, S. A.; Appel, A. M.; Gagliardi, L.; Lu, C. C. A Bimetallic Nickel–Gallium Complex Catalyzes CO_2 Hydrogenation via the Intermediacy of an Anionic d^{10} Nickel Hydride. *J. Am. Chem. Soc.* **2017**, *139*, 14244; (d) Schieweck, B. G.; Westhues, N. F.; Klankermayer, J. A Highly Active Non-Precious Transition Metal Catalyst for the Hydrogenation of Carbon Dioxide to Formates. *Chem. Sci.* **2019**, *10*, 6519.

15. For selected leading references see: (a) Watari, R.; Kayaki, Y.; Hirano, S. i.; Matsumoto, N.; Ikariya, T. Hydrogenation of Carbon Dioxide to Formate Catalyzed by a Copper/1,8-Diazabicyclo[5.4.0]undec-7-ene System. *Adv. Synth. Catal.* **2015**, *357*, 1369; (b) Zall, C. M.; Linehan, J. C.; Appel, A. M. A Molecular Copper Catalyst for Hydrogenation of CO_2 to Formate. *ACS Catal.* **2015**, *5*, 5301; (c) Zall, C. M.; Linehan, J. C.; Appel, A. M. Triphosphine-Ligated Copper Hydrides for CO_2 Hydrogenation: Structure, Reactivity, and Thermodynamic Studies.

J. Am. Chem. Soc. **2016**, *138*, 9968; (d) Chaudhary, K.; Trivedi, M.; Masram, D. T.; Kumar, A.; Kumar, G.; Husain, A.; Rath, N. P. A Highly Active Copper Catalyst for the Hydrogenation of Carbon Dioxide to Formate Under Ambient Conditions. *Dalton Trans.* **2020**, *49*, 2994.
16. (a) Alberico, E.; Sponholz, P.; Cordes, C.; Nielsen, M.; Drexler, H.-J.; Baumann, W.; Junge, H.; Beller, M. Selective Hydrogen Production from Methanol with a Defined Iron Pincer Catalyst under Mild Conditions. *Angew. Chem. Int. Ed.* **2013**, *52*, 14162; (b) Bielinski, E. A.; Förster, M.; Zhang, Y.; Bernskoetter, W. H.; Hazari, N.; Holthausen, M. C. Base-Free Methanol Dehydrogenation Using a Pincer-Supported Iron Compound and Lewis Acid Co-catalyst. *ACS Catal.* **2015**, *5*, 2404; (c) Curley, J. B.; Bernskoetter, W. H.; Hazari, N. Additive-Free Formic Acid Dehydrogenation Using a Pincer-Supported Iron Catalyst. *ChemCatChem* **2020**, *12*, 1934; (d) Curley, J. B.; Smith, N. E.; Bernskoetter, W. H.; Ertem, M. Z.; Hazari, N.; Mercado, B. Q.; Townsend, T. M.; Wang, X. Understanding the Reactivity and Decomposition of a Highly Active Iron Pincer Catalyst for Hydrogenation and Dehydrogenation Reactions. *ACS Catal.* **2021**, *11*, 10631.
17. Jeffrey, J. C.; Rauchfuss, T. B. Metal Complexes of Hemilabile Ligands. Reactivity and Structure of Dichlorobis(o-(diphenylphosphino)anisole)ruthenium(II). *Inorg. Chem.* **1979**, *18*, 2658.
18. (a) Bader, A.; Lindner, E. Coordination Chemistry and Catalysis with Hemilabile Oxygen-Phosphorus Ligands. *Coord. Chem. Rev.* **1991**, *108*, 27; (b) Slone, C. S.; Weinberger, D. A.; Mirkin, C. A. In *Prog. Inorg. Chem.* 1999; Vol. 48, p 233; (c) Braunstein, P.; Naud, F. Hemilability of Hybrid Ligands and the Coordination Chemistry of Oxazoline-Based Systems. *Angew. Chem. Int. Ed.* **2001**, *40*, 680; (d) Van Der Vlugt, J. I. Cooperative Catalysis with First-Row Late Transition Metals. *Eur. J. Inorg. Chem.* **2012**, 363; (e) Adams, G. M.; Weller, A. S. POP-type Ligands: Variable Coordination and Hemilabile Behaviour. *Coord. Chem. Rev.* **2018**, *355*, 150; (f) Blacquiere, J. M. Structurally-Responsive Ligands for High-Performance Catalysts. *ACS Catal.* **2021**, *11*, 5416.
19. (a) Springman, E. B.; Angleton, E. L.; Birkedal-Hansen, H.; Van Wart, H. E. Multiple Modes of Activation of Latent Human Fibroblast Collagenase: Evidence for the Role of a Cys73 Active-Site Zinc Complex in Latency and a "Cysteine Switch" Mechanism for Activation. *Proc. Natl. Acad. Sci. U.S.A* **1990**, *87*, 364; (b) Van Wart, H. E.; Birkedal-Hansen, H. The Cysteine Switch: A Principle of Regulation of Metalloproteinase Activity with Potential Applicability to the Entire Matrix Metalloproteinase Gene Family. *Proc. Natl. Acad. Sci. U.S.A* **1990**, *87*, 5578; (c) Ding, S.; Ghosh, P.; Darensbourg, M. Y.; Hall, M. B. Interplay of Hemilability and Redox Activity in Models of Hydrogenase Active Sites. *Proc. Natl. Acad. Sci. U.S.A* **2017**, *114*, E9775.
20. (a) Sacconi, L.; Bertini, I. Low- and High-Spin Five-Coordinate Cobalt(II) and Nickel(II) Complexes with Tris(2-diphenylphosphinoethyl)amine. *J. Am. Chem. Soc.* **1968**, *90*, 5443; (b) Sacconi, L.; Bertini, I.; Mani, F. Five-Coordination with "Hybrid" Ligands. II. Nickel(II) Complexes with Polyfunctional Arsenic-Containing Ligands. *Inorg. Chem.* **1968**, *7*, 1417; (c) Sacconi, L.; Morassi, R. Five-Co-Ordination with 'Hybrid' Ligands. Part V. Cobalt(II) and Nickel(II) Complexes with Tetradentate Ligands Containing Nitrogen and Phosphorus or Arsenic as Donor Atoms. *J. Chem. Soc. A* **1969**, *1969*, 2904; (d) Morassi, R.; Sacconi, L. Five-Co-Ordination with 'Hybrid' Ligands. Part VI. Cobalt(II) and Nickel(II) Complexes with a Quadridentate Tripod Ligand Having a NOPP Donor Set. *J. Chem. Soc. A* **1971**, 492; (e) MacBeth, C. E.; Harkins, S. B.; Peters, J. C. Synthesis and Characterization of Cationic Iron Complexes Supported by the Neutral Ligands NP^iPr_3, $NArP^iPr_3$, and NS^tBu_3. *Can. J. Chem.* **2005**, *83*, 332; (f) Peruzzo, V.; Pretzsch, C.; Tisato, F.; Porchia, M.; Refosco, F.; Marzano, C.; Gandin, V.; Schiller, E.; Walther, M.; Pietzsch, H. J. Synthesis and Characterization of Novel Tetrahedral Copper(I) Complexes Comprising Tridentate PNP-Aminodiphosphines and Tetradentate PN(X)P-Substituted Aminodiphosphines (X = O, S). *Inorg. Chim. Acta* **2012**, *387*, 163; (g) Gradiski, M. V.; Tsui, B. T. H.; Lough, A. J.; Morris, R. H. PNN′ & P_2NN' Ligands via Reductive Amination with Phosphine Aldehydes: Synthesis and Base-Metal Coordination Chemistry. *Dalton Trans.* **2019**, *48*, 2150; (h) Deolka, S.; Tarannam, N.; Fayzullin, R. R.; Kozuch, S.; Khaskin, E. Unusual Rearrangement of Modified PNP Ligand Based Ru Complexes Relevant to Alcohol Dehydrogenation Catalysis. *Chem. Commun.* **2019**, *55*, 11350.
21. Wedal, J. C.; Virtue, K. B.; Bernskoetter, W. H.; Hazari, N.; Mercado, B. Q. Iron Catalysts Supported by a PNP Ligand with an Additional Hemilabile Donor for CO_2 Hydrogenation. *ACS Catal.* **2024**, *14*, 13903.
22. The TONs presented in Figure 1 are the maximum obtained by a specific catalyst regardless of the reaction conditions. Under the same reaction conditions **I** and **II** give similar TONs.
23. Rima, G.; Satgé, J.; Fatome, M.; Laval, J. D.; Sentenac-Roumanou, H.; Lion, C.; Lazraq, M. Synthèse et Activité Radioprotectrice de Nouveaux Trithiagermatranes, Trithiasilatranes, Oxyde et Sulfure Germaniés à Substituant Chlorhydrate de Cystéamine et N(2-thioéthyl)-1,3-diaminopropane. *Eur. J. Med. Chem.* **1991**, *26*, 291.
24. Werkmeister, S.; Junge, K.; Wendt, B.; Alberico, E.; Jiao, H.; Baumann, W.; Junge, H.; Gallou, F.; Beller, M. Hydrogenation of Esters to Alcohols with a Well-Defined Iron Complex. *Angew. Chem. Int. Ed.* **2014**, *53*, 8722.
25. Wang, Q. Q.; Begum, R. A.; Day, V. W.; Bowman-James, K. Sulfur, Oxygen, and Nitrogen Mustards: Stability and Reactivity. *Org. Biomol. Chem.* **2012**, *10*, 8786.

26. Nguyen, D. H.; Trivelli, X.; Capet, F.; Paul, J. F.; Dumeignil, F.; Gauvin, R. M. Manganese Pincer Complexes for the Base-Free, Acceptorless Dehydrogenative Coupling of Alcohols to Esters: Development, Scope, and Understanding. *ACS Catal.* **2017**, *7*, 2022.
27. Fu, S.; Shao, Z.; Wang, Y.; Liu, Q. Manganese-Catalyzed Upgrading of Ethanol into 1-Butanol. *J. Am. Chem. Soc.* **2017**, *139*, 11941.
28. (a) Elangovan, S.; Topf, C.; Fischer, S.; Jiao, H.; Spannenberg, A.; Baumann, W.; Ludwig, R.; Junge, K.; Beller, M. Selective Catalytic Hydrogenations of Nitriles, Ketones, and Aldehydes by Well-Defined Manganese Pincer Complexes. *J. Am. Chem. Soc.* **2016**, *138*, 8809; (b) Tondreau, A. M.; Boncella, J. M. The Synthesis of PNP-Supported Low-Spin Nitro Manganese(I) Carbonyl Complexes. *Polyhedron* **2016**, *116*, 96.
29. (a) Petriček, S.; Demšar, A. Syntheses and Crystal Structures of Manganese, Nickel and Zinc Chloride Complexes with Dimethoxyethane and di(2-methoxyethyl) Ether. *Polyhedron* **2010**, *29*, 3329; (b) Antico, E.; Leutzsch, M.; Wessel, N.; Weyhermüller, T.; Werlé, C.; Leitner, W. Selective Oxidation of Silanes into Silanols with Water Using [$MnBr(CO)_5$] as a Precatalyst. *Chem. Sci.* **2023**, *14*, 54; (c) Goodall, J. C.; Sajjad, M. A.; Thompson, E. A.; Page, S. J.; Kerrigan, A. M.; Jenkins, H. T.; Lynam, J. M.; Macgregor, S. A.; Weller, A. S. In Crystallo Lattice Adaptivity Triggered by Solid-Gas Reactions of Cationic Group 7 Pincer Complexes. *Chem. Commun.* **2023**, *59*, 10749; (d) Yuan, G.-J.; Pan, X.-W.; Chen, L.; Chen, C.; Ren, X.-M. Supramolecular Crystals of Mn(15-crown-5)($MnCl_4$)(DMF) with Dielectric Phase Transition, High Quantum Yield and Phase Transition-Induced Luminescence Enhancement Behavior. *Dalton Trans.* **2024**, *53*, 2687.
30. (a) Balaraman, E.; Gnanaprakasam, B.; Shimon, L. J. W.; Milstein, D. Direct Hydrogenation of Amides to Alcohols and Amines under Mild Conditions. *J. Am. Chem. Soc.* **2010**, *132*, 16756; (b) Filonenko, G. A.; Conley, M. P.; Copéret, C.; Lutz, M.; Hensen, E. J. M.; Pidko, E. A. The Impact of Metal–Ligand Cooperation in Hydrogenation of Carbon Dioxide Catalyzed by Ruthenium PNP Pincer. *ACS Catal.* **2013**, *3*, 2522; (c) Kallmeier, F.; Irrgang, T.; Dietel, T.; Kempe, R. Highly Active and Selective Manganese C=O Bond Hydrogenation Catalysts: The Importance of the Multidentate Ligand, the Ancillary Ligands, and the Oxidation State. *Angew. Chem. Int. Ed.* **2016**, *55*, 11806; (d) Kar, S.; Goeppert, A.; Kothandaraman, J.; Prakash, G. K. S. Manganese-Catalyzed Sequential Hydrogenation of CO_2 to Methanol via Formamide. *ACS Catal.* **2017**, *7*, 6347.
31. (a) Di Vaira, M.; Ghilardi, C. A.; Sacconi, L. Synthesis and Structural Characterization of Some Nitrosyl Complexes of Iron, Cobalt, and Nickel with Poly(tertiary phosphines and arsines). *Inorg. Chem.* **1976**, *15*, 1555; (b) Cecconi, F.; Dapporto, P.; Midollini, S.; Sacconi, L. Synthesis, Characterization, and Structure of the Complex (η^3-cyclo-triphosphorus)(tris(2-diphenylphosphinoethyl)amine)cobalt. *Inorg. Chem.* **1978**, *17*, 3292; (c) Cecconi, F.; Ghilardi, C. A.; Innocenti, P.; Midollini, S.; Orlandini, A. Reductive Intramolecular Hydrogen Transfer in a d^8 Metal Hydride Promoted by Carbon Monoxide Addition. An Experimental Study and its Theoretical Implications. *Inorg. Chem.* **1984**, *23*, 922.

TOC Graphic

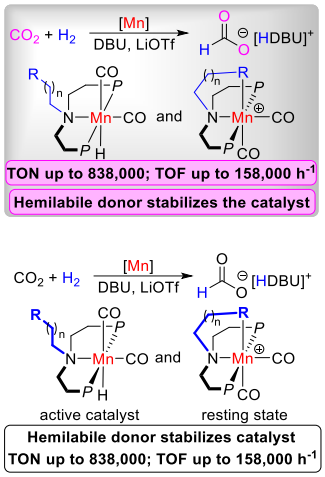
CO2 + H2
[Mn]
DBU, LiOTf
[HDBU]+
and
TON up to 838,000; TOF up to 158,000 h-1
Hemilabile donor stabilizes the catalyst

CO2 + H2
[Mn]
DBU, LiOTf
[HDBU]+
and
active catalyst
resting state
Hemilabile donor stabilizes catalyst
TON up to 838,000; TOF up to 158,000 h-1